PLASMA RESEARCH

CASE INSTITUTE OF TECHNOLOGY

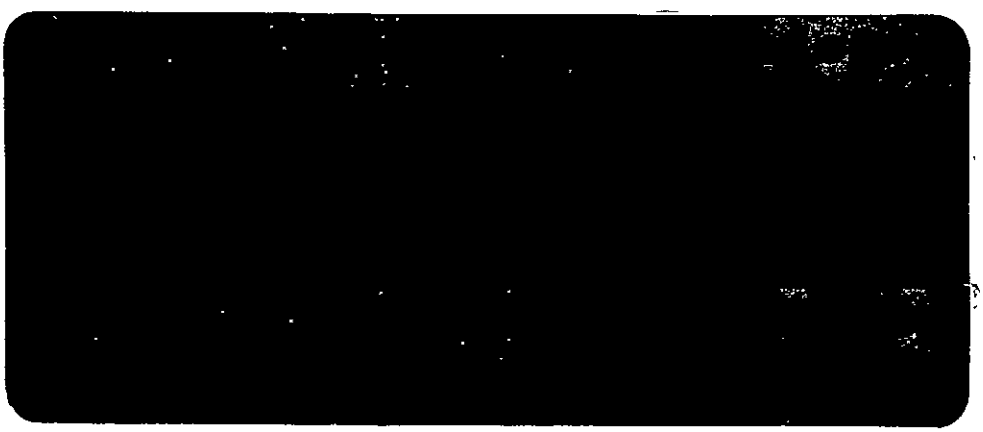

UNIVERSITY CIRCLE • CLEVELAND 6, OHIO

A WIDE-BAND DICKE RADIOMETER

by

Ali T. Alper

Technical Report No. A-45

June, 1966

This work was supported by the National Aeronautics and Space Administration.

A Thesis submitted to Case Institute of Technology in partial fulfillment of the requirements for the Degree of Master of Science.

ABSTRACT

A wide-band Dicke radiometer capable of operating in the frequency range 2.6 to 14 KMC is constructed. The operation of the radiometer is explained with special emphasis on the accomplishment of such an extremely wide bandwidth. Calibration of the radiometer is carried out within the 2.6 to 9 KMC frequency range using three different noise sources. As an application of this wide-band receiver, electron cyclotron resonance intensity measurements in a plasma are made. ( )

ACKNOWLEDGMENTS

The author wishes to express his gratitude to Professor Osman K. Mawardi, for the suggestion of the thesis and his continuing guidance. He would also like to thank Dr. A. M. Ferendeci, and especially to Mr. R. O. Shaffner for their helpful suggestions in the completion of the project.

Thanks is also due to Mrs. Martha S. Dybas and Miss Jeanette Yount for their competent typing of the manuscript.

The financial support was provided in part by Nato Ilim Burslari Komitesi (Nato Scientific Fellowship Committee of Turkey), and the National Aeronautics and Space Administration.

TABLE OF CONTENTS

LIST OF ILLUSTRATIONS

CHAPTER I

INTRODUCTION

All objects above absolute zero temperature radiate energy as electromagnetic waves. The intensity of radiation, when thermodynamic equilibrium prevails, is given by the Plank's radiation formula and depends on the temperature of the body. If the object in question is a "blackbody", radiated power (P) per cycle per second is related to the temperature (T) as,

$$\frac{P}{\Delta f} = kT \qquad (1)$$

where Δf is the frequency bandwidth considered, and k is the Boltzmann's constant.

The detection of weak thermal radiation, or similar signals, at the radio and microwave frequencies is limited by the internal noise of the receiving equipment. For this purpose special techniques like "radiometry" are required. Radiometry makes use of a radiometer which is a very sensitive power detecting device, that measures electromagnetic energy considered as thermal radiation. A radiometer has to be extremely sensitive, since, for example an object at a temperature of 1000°K has an equivalent radiative power of about 1.4×10^{-20} watts/cycle/sec., according to equation (1). Measurements of such a small signal undoubtedly requires high

sensitivity equipment.

Radiometers can be classified, mainly, in two groups:

1. Subtraction type
2. Multiplier type.

In most of the early work on weak thermal radiation studies, subtraction type radiometers have been used.[7,19] Figure 1 shows the main parts of such an instrument. The received signal is amplified and detected. After the detector a subtractor, a low-pass filter, and an output meter are placed. A known d.c. voltage is fed into the subtractor to insure that the output meter reads zero when there is no signal at the receiver input. The sensitivities reached with this type of instrumentation are adequate, whenever the fluctuations and drift within the receiver components are negligible. Unfortunately this is not true with the conventional vacuum tube receivers, and the multiplication type radiometers are preferred for weak thermal radiation measurements because of their superior sensitivities.

The first multiplier type radiometer was built in 1946 by Dicke.[4] The main components of the Dicke type radiometer are shown in Figure 2. In this device, the incoming signal is modulated to achieve the high sensitivity. The signal is detected after conversion to intermediate frequency by beating it against a local oscillator within the mixer. Using this type of rediometer Dicke was able to detect a temperature change of about 0.5°K, and used it

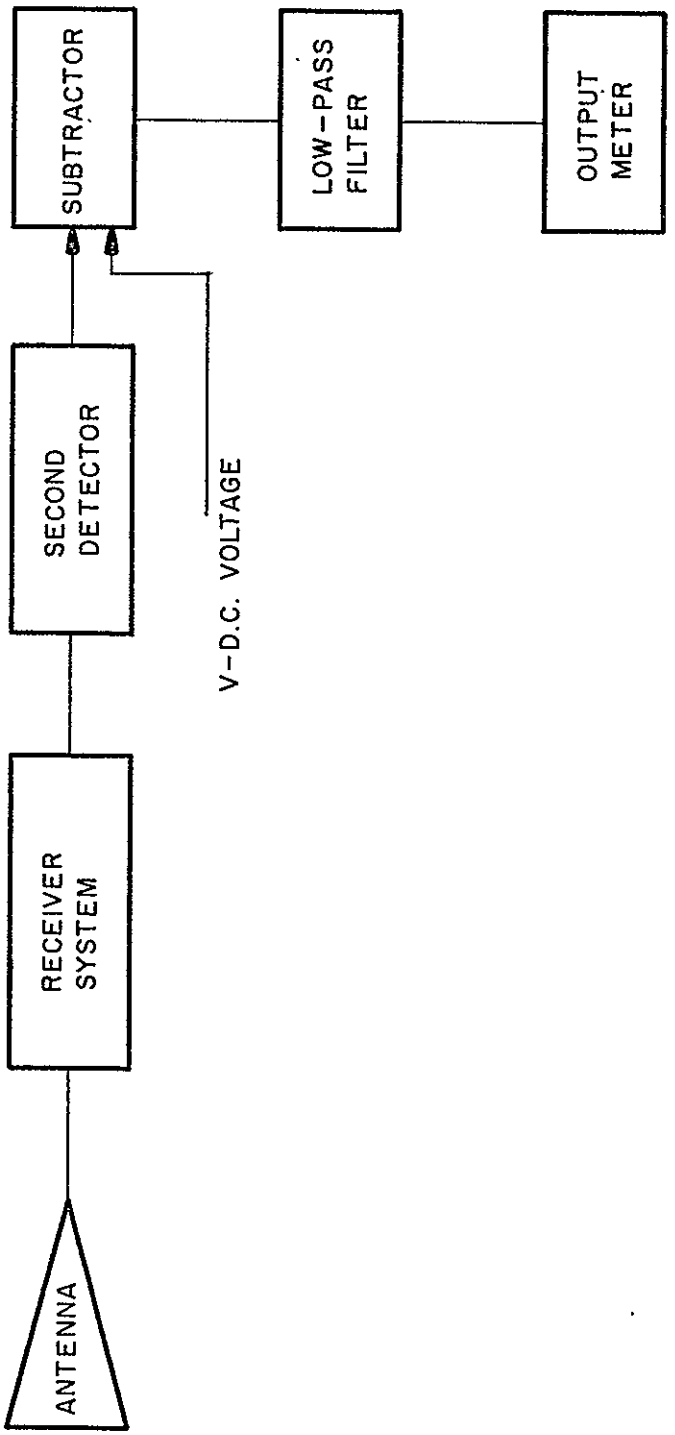

Fig. 1. A Subtraction-Type Radiometer

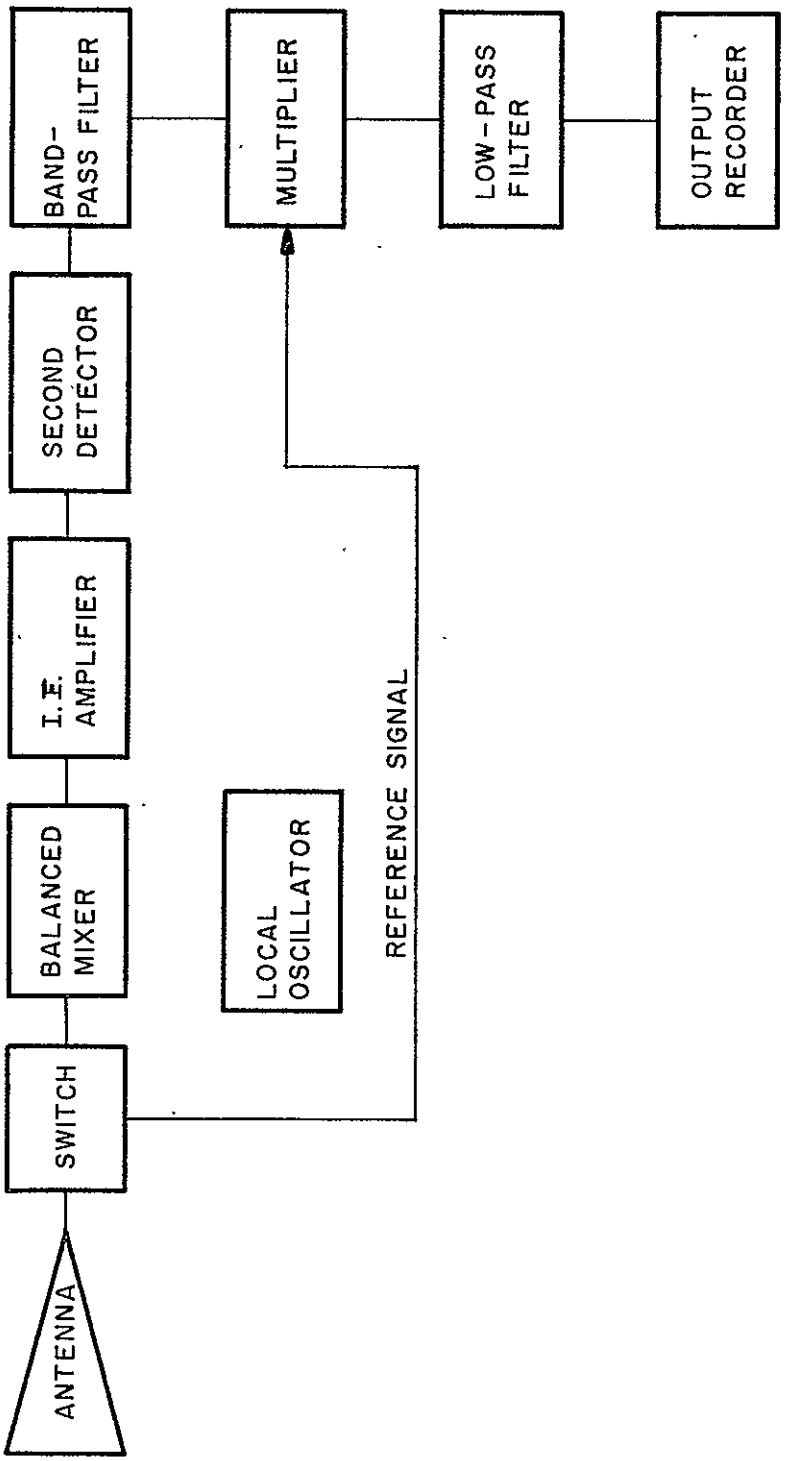

Fig. 2 A Dicke Type Radiometer

in measurements of thermal radiation from the moon, and the sun.

Since 1946, several people working with weak thermal radiation measurements have made use of similar circuitry shown in Figure 2. Its use have been largely employed in radio-astronomy studies.[4,11] This type of radiometer has also been used in laboratory plasma measurements.[1,15,22]

After the discovery of traveling wave-tubes, radiometers involving TWT have also been built.[5,21] The block diagram of a traveling-wave tube radiometer is shown in Figure 3. The principle of operation is the same as the Dicke radiometer, except that detection takes place at the microwave frequency level. Sensitivities of TWT radiometers are much superior to those which involve an i.f. amplifier since low noise-figure, and high gain traveling-wave tubes are available. Temperature changes of 0.01°K has been detected in this manner, using traveling-wave tubes.[5]

The main concern of this work has been the construction of a Dicke type radiometer which is capable of operating in a very wide frequency bandwidth (2.6 to 14 KMC). Ridged-waveguide components have been constructed in order to obtain such a broad-bandwidth receiver system. A double-ridged waveguide balanced mixer, modulating switch, and directional coupler have been built. In order to make the maximum use of the radiometer, waveguide transitions from the double-ridged to the conventional "S" , and "X"

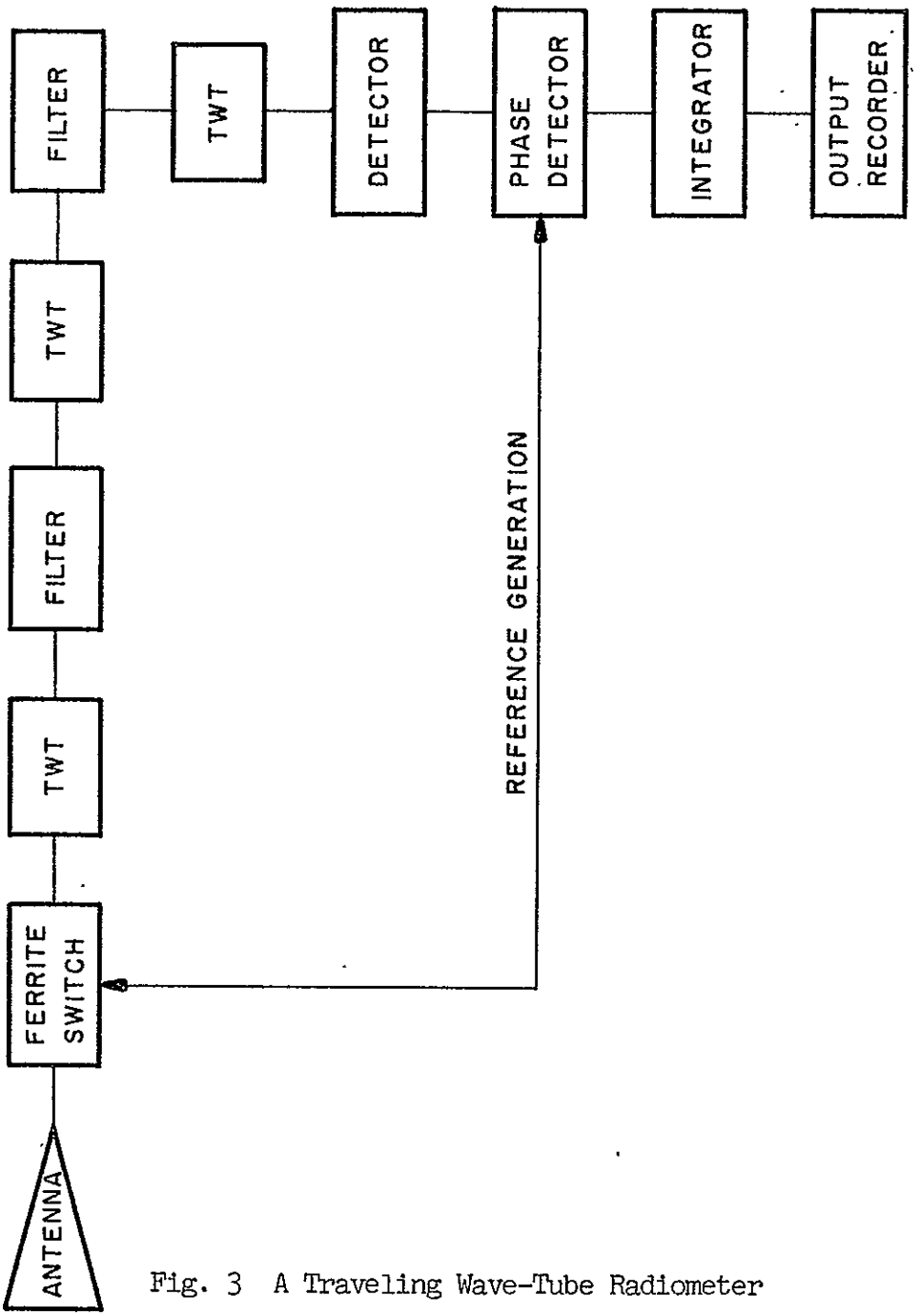

Fig. 3 A Traveling Wave-Tube Radiometer

band have also been developed and constructed.

For the receiver part of the radiometer, a low-noise (noise figure of 3 db) 30 MC tuned i.f. amplifier has been designed with a gain of about 90 db, and 1.5 MC bandwidth.

The calibration of the radiometer is carried out using fluorescent and argon noise sources located inside of an S-band waveguide. After the calibration process, as one immediate application of the radiometer, cyclotron radiation intensity measurements have been obtained from an argon discharge tube located inside of a magnet.

CHAPTER II

THEORY OF OPERATION

Radiometers are used in weak thermal radiation measurements, and therefore sensitivity is a crucial factor. Before computing the minimum detectable signal of a Dicke type radiometer, it will be helpful to summarize several thresholds which affect the sensitivity of a radiometer.[21]

There are mainly four thresholds which influence the sensitivity:

1. Thresholds due to internal noise of the receiver,
2. Thresholds due to gain fluctuations,
3. Thresholds due to impedance modulation, and
4. Thresholds due to the receiving antenna.

Main contributions to the internal noise come from the i.f. amplifier, balanced mixer, and the local oscillator. The crystals in the balanced mixer arms have an intrinsic noise, which is introduced to the system through the i.f. amplifier. Any mismatch of the mixer crystals will cause local oscillator noise to be amplified. I.F. amplifier input impedance and the vacuum tubes in the amplifier are also sources of noise consequently a low-noise i.f. amplifier is essential to a radiometer. The other contributions associated with this threshold can be caused by the detectors, and the filters used. Even though the sensitivity of a radiometer is independent of the

detector used, the power output is very much dependent on it.[20] However, the type of low-pass filter used can affect the sensitivity considerably. For example, a critically damped low-pass filter provides an optimum sensitivity.[21]

The i.f. amplifier in a radiometer operates with a very high gain, in the order of 10^5 - 10^6. Any small variation in the gain will cause severe fluctuations of the output meter. Possible sources of variation can be due to change in the line voltage, ambient temperature drift of the tubes, etc.. There are also fluctuations in the conversion gain and the intrinsic noise of the crystals within the mixer. In order to reduce gain fluctuations the amplitude modulation of the incoming signal should be at a frequency higher than the maximum significant component of gain fluctuations spectrum. In the switching or amplitude modulation process, if the reference source and antenna temperature differ greatly, there will exist a threshold because of temperature fluctuations. However, a stable comparison source can reduce this factor.[21]

The third threshold is attributed to the impedance modulation. Amplitude modulation of the signal creates this difficulty. However, if modulation takes place in a systematic manner, effects of impedance modulation on the sensitivity are negligible.

The last threshold mentioned above is established by the characteristics of the antenna. The sizes of the antenna and the back lobes created, pose problems in most of the astronomical

studies. Factors involved in the antenna threshold will not have significant effects in our measurements, since the radiometer will be used mostly in conjunction with highly directive horns.

The thresholds explained above point out the purpose of different parts of a Dicke radiometer (Fig. 2): a) In order to reduce the effective internal noise measured on the output meter, a low-pass filter is placed just before the output recorder. b) Gain fluctuations in the receiver are reduced by amplitude modulation of the signal. c) After the detection process, signal is fed through a bandpass filter centered about the modulation frequency, which filters out the white-noise contributed internally.

The expression for the minimum detectable signal of a radiometer, can be calculated using diagram of Figure 4. In the derivations correlation technique is used, and also the "ergodic" theorem is assumed. This theorem simply states that; "the statistical ensemble averages can be replaced by the time averages." Mathematical derivations are carried out in Appendix I with the following assumptions:[9]

1. Signal $s(t)$, and noise $n(t)$ have independent stationary Gaussian amplitude distributions with zero means and average powers of σ_s^2 and σ_n^2 respectively.

2. Signal and noise have uniform spectral densities over the frequency range $f_1 - \frac{\alpha}{2}$ to $f_1 + \frac{\alpha}{2}$.

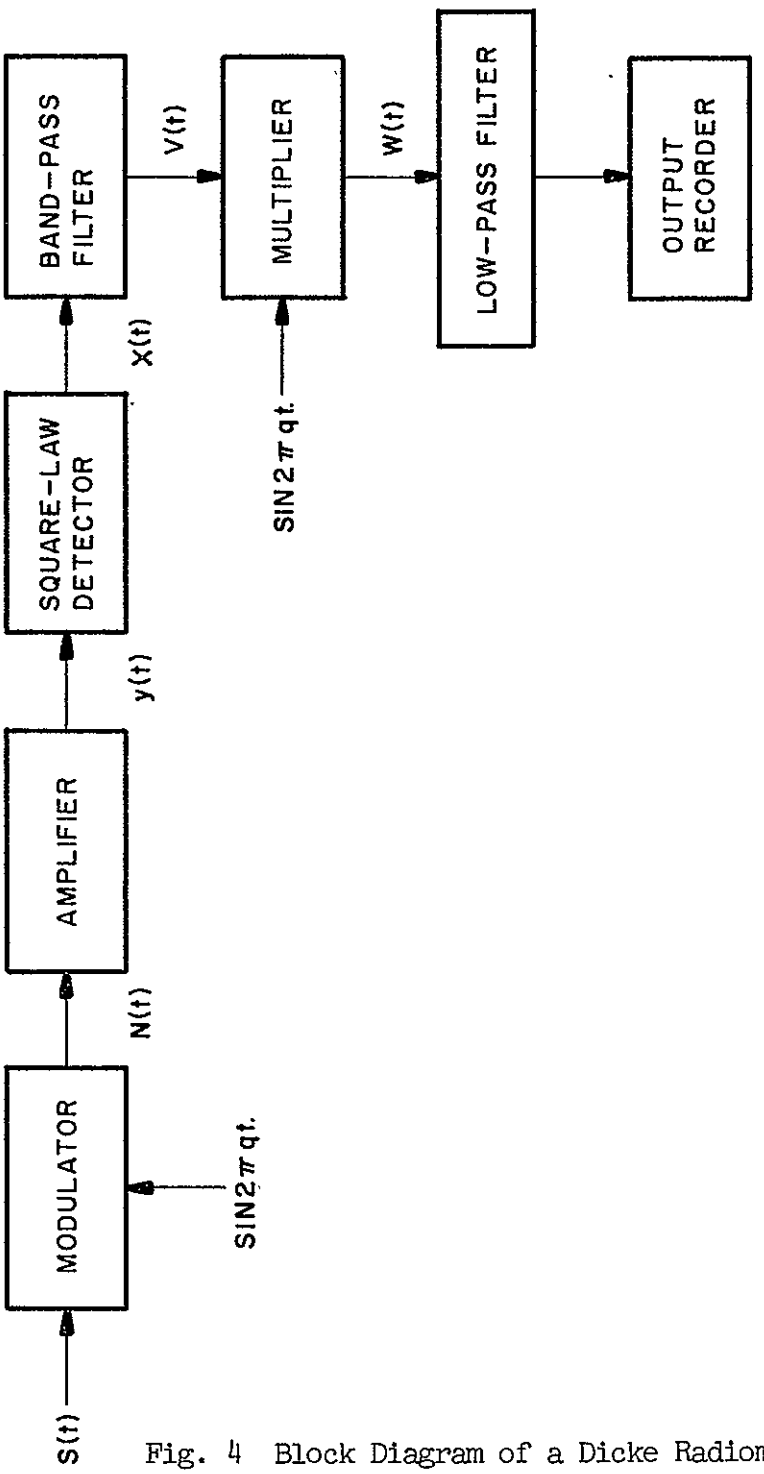

Fig. 4 Block Diagram of a Dicke Radiometer

3. The modulator has a frequency q , and does not affect the noise.

4. The band-pass filter has uniform response from $q - \frac{\beta}{2}$ to $q + \frac{\beta}{2}$ cps where β is the bandwidth of the filter.

5. The low-pass filter has a uniform response over the range 0 to γ cps.

6. The i.f. amplifier is tuned at a frequency f_1 cps , has a bandwidth of α cps , an produces linear gain.

As shown in Appendix I, the output signal to noise ratio of this type of radiometer is,

$$\left(\frac{S}{N}\right)_o = \frac{\frac{\sigma_s^4}{16}}{\frac{17}{32}\sigma_s^4 + \frac{3}{2}\sigma_s^2\sigma_n^2 + 2\sigma_n^4}\left(\frac{\alpha}{\gamma}\right) . \qquad (2)$$

For weak signals $\sigma_s^2 << \sigma_n^2$, and therefore,

$$\left(\frac{S}{N}\right)_o = \frac{\sigma_s^4}{32\sigma n^4}\left(\frac{\alpha}{\gamma}\right) . \qquad (3)$$

When the worst possible case of output signal to noise ratio equal to one, $\left(\frac{S}{N}\right)_o = 1$, is considered, the expression for the minimum detectable signal in terms of the input noise power reduces to,

$$\sigma_{md}^2 = 4\sqrt{2}\,\sigma_n^2\sqrt{\frac{\gamma}{\alpha}} . \qquad (4)$$

The expression in equation (4) is dependent on the bandwidths of the low-pass filter as well as of the i.f. amplifier. The value of γ for the filter can be made as small as possible. However, the amplifier bandwidth has to be selected for an optimum sensitivity. When the i.f. bandwidth is made too large, the amplifier gain will drop because of the constant gain bandwidth product, and the power at the radiometer output will be small.

The minimum detectable signal of a radiometer also depends on the type of modulation, and on the reference signal fed into the multiplier (Figure 4). Derivation of equation (4) is carried out assuming sinusoidal modulation, and sinusoidal reference signal. When square-wave modulation, and square-wave reference signal is produced, the power output increases by a factor of 4 to give,[23]

$$\sigma_{md}^2 = \sqrt{2}\,\sigma_n^2 \sqrt{\frac{\gamma}{\alpha}} \qquad (5)$$

Instead of expressing minimum detectable signal of a radiometer, the least detectable temperature change can also be specified. When a critically damped low-pass filter is used,[4,11]

$$\Delta T = kTa\, F\left(\frac{\gamma}{\alpha}\right)^{1/2}$$

where α and γ are the bandwidths specified before,

F is the overall receiver noise figure, expressed as a power ratio,

ΔT, the temperature fluctuations of the output meter,

Ta, the temperature of the comparison source, and

k is a constant.

The constant k is called the operator's constant. It will vary for different radiometer circuits, depending specifically on the type of filters and the switching process used.[11]

CHAPTER III

DESCRIPTION OF THE APPARATUS

The radiometer which has been constructed is the Dicke radiometer shown in Fig. 2, which operates over the broadband frequency range 2.6 to 14 KMC. Over such a wide frequency bandwidth, it is no longer possible to use standard waveguide components for the microwave frequency section of the receiver. However construction of ridged-waveguide instruments with suitable guide dimensions, makes it possible to operate the receiver in the desired frequency spectrum.

The pictures of the experimental setup for the radiometer are shown in Figures 5 and 6. The antenna, at the input of the receiver, is a waveguide horn with a transition from the X- or the S-Band conventional waveguide to the double-ridge guide. Behind the antenna a switch is located for amplitude modulation of the incoming signal. This switch is built also from double-ridge waveguide , and the modulation is accomplished by driving a resistive card in and out of the guide using a motor. On the upper part of the switching waveguide a photo conductor is placed to supply the reference signal synchronized with the modulation process.

The microwave switch is followed by a double-ridge balanced mixer. The incoming signal is fed into the "E" plane while the

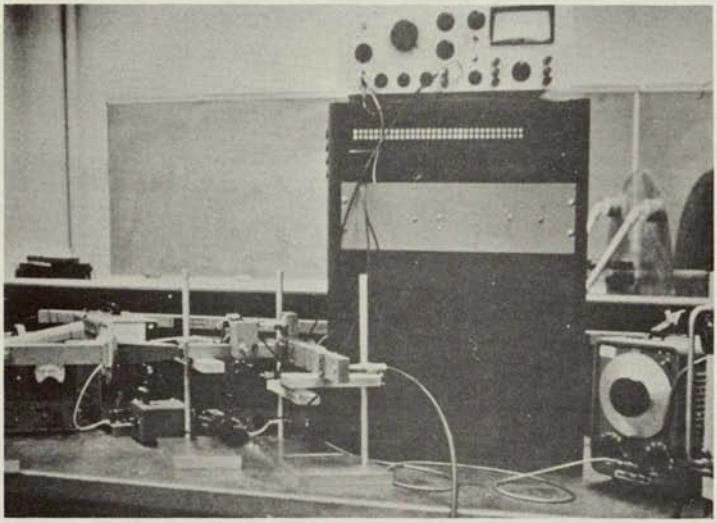

Figure 5. Photograph of Equipment

NOT REPRODUCIBLE

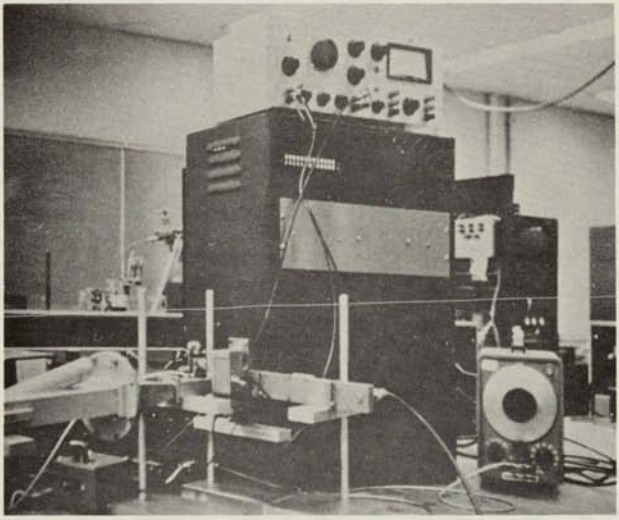

Figure 6. Photograph of Equipment

local oscillator is connected to the "H" plane of the mixer - also referred to as the magic "T" (Figure 7). The magic "T" provides frequency conversion of the incoming signal from the microwave to the intermediate frequency by beating of the local oscillator against the signal. The balanced arms of the mixer are equipped with microwave crystals, and the output from these crystals is applied to an i.f. amplifier. The i.f. amplifier is tuned at 30 MC, and the input circuit of the amplifier is designed in such a way as to cancel the local oscillator output noise.

Following the i.f. amplifier, a square-law detector is connected, and the output of the detector is applied to a phase lock-in amplifier system (LIA). The phase lock-in system is composed of a band-pass filter, a multiplier circuit for demodulation, and an R-C low-pass filter.

The (LIA) is essentially a phase sensitive detecting instrument. The signal to be measured is applied to the "INPUT" terminals. A potentiometer is located at the input in order to pick out any desired fraction of the incoming signal. The signal level control terminals are followed by an amplifier tunable to the desired frequency to be studied. The output of the amplifier is applied to a phase-sensitive detector. This detector is essentially a mixer diode, and the demodulation of the signal is accomplished within the detector by the application of a reference voltage to the diode. The reference signal is at the modulation frequency, and at the

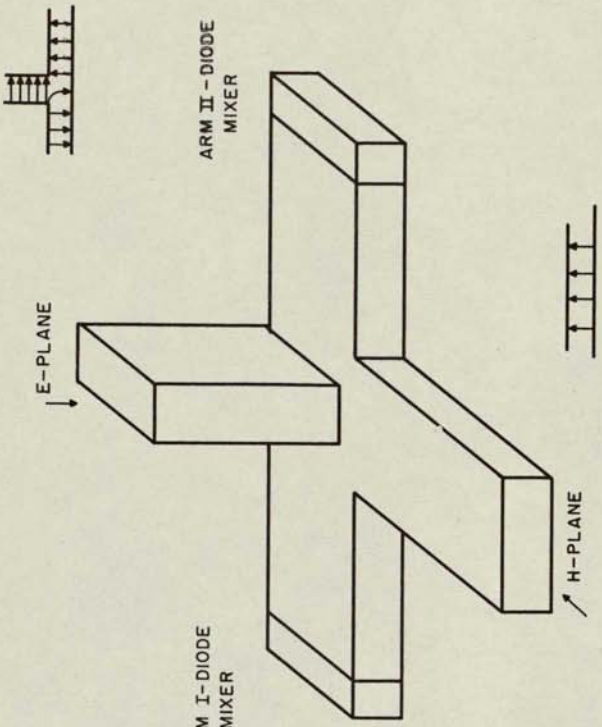

Fig. 7 A Magic "T"

output of the phase detector sum and difference of the input and the reference frequencies are obtained. The difference of two of these signal frequencies is zero, and the amplitude of this D-C voltage is dependent upon the cosine of the relative phases of the signal and the reference waveforms. The contribution from the sum of two frequencies is eliminated with a low-pass filter following the phase detector. The low-pass filter is an R-C circuit whose time constant is adjustable to as high as 10 seconds. The zero frequency D.C. output of the low-pass filter is further amplified. The output terminals of the lock-in amplifier are internally connected to a galvanometer, and there are provisions for measurements with any type of recorder.

The critical part of this wideband radiometer is the design and construction of the ridged-waveguide components. Following the construction of two prototypes, the dimensions and the shape of the balanced mixer is determined for optimum operation over the range 2.6 to 14 KMC. Pictures of some ridged-guide instruments are shown in Fig. 8. In order to obtain adequate information about the operation of the ridged-waveguide components, a slotted line is constructed in addition to the essential parts such as the switch, the balanced mixer, the coaxial to ridge transitions, a directional coupler, a ridged-guide termination, and two horns from the X- and S-Band to the double-ridge.

The dimensions of the double-ridge waveguide used are shown in

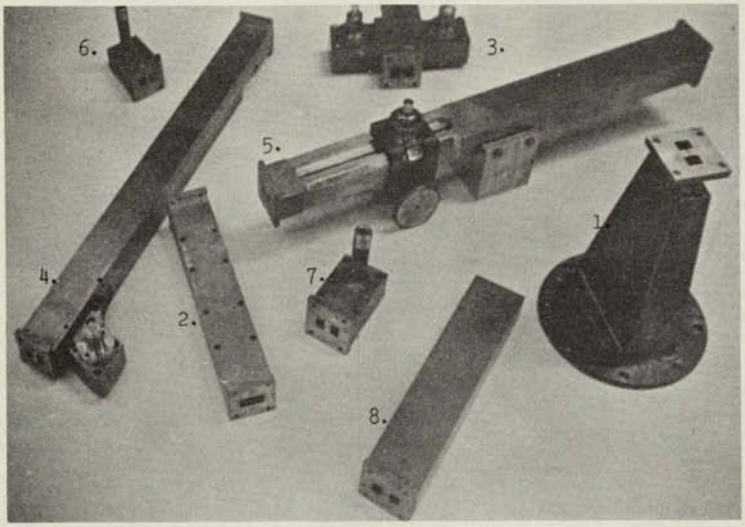

Figure 8. Ridged-Waveguide Instruments

1. S-Band to ridge transition.
2. X-Band to ridge transition.
3. Double-ridge balanced mixer.
4. Double-ridge directional coupler.
5. Slotted-line.
6. Coaxial to ridge guide adapter.
7. Coaxial to ridge guide adapter.
8. Double-ridge termination.

Fig. 9. The width and height of the guide are selected to be identical to the dimensions of a regular X-Band waveguide. The chosen cross-section provides the extended bandwidth capability. The cutoff-frequencies of a rectangular X-Band waveguide for the TE_{10} and the TE_{20} mode are,

$$f_{c,10} \cong 6.67 \text{ KMC}$$
$$f_{c,20} \cong 13.34 \text{ KMC} \qquad (7)$$

The cutoff frequency for the TE_{10} mode is reduced by a factor of about 2.57 with the ridge gap of 0.040". On the other hand, fortunately, the cutoff frequency for the TE_{20} mode is increased by a factor of about 1.2. The cutoff frequencies of the double-ridged waveguide of Fig. 9 are,

$$f'_{c,10} \cong 2.59 \text{ KMC}$$
$$f'_{c,20} \cong 16 \text{ KMC} \qquad (8)$$

Therefore, in the TE_{10} mode it is possible to operate the double-ridged guide from 2.6 to 14 KMC. Such an extended bandwidth sacrifices the power handling capacity of the ridged waveguides. Also, the attenuation is higher and the guide characteristic impedance is diminished by a factor about 6. [2,8,12,13]

A picture of the waveguide switch is shown in Fig. 10. In the center of the guide, a slot of width 0.090" is cut. Since the width of the ridge is three times the width of the slot in that region,

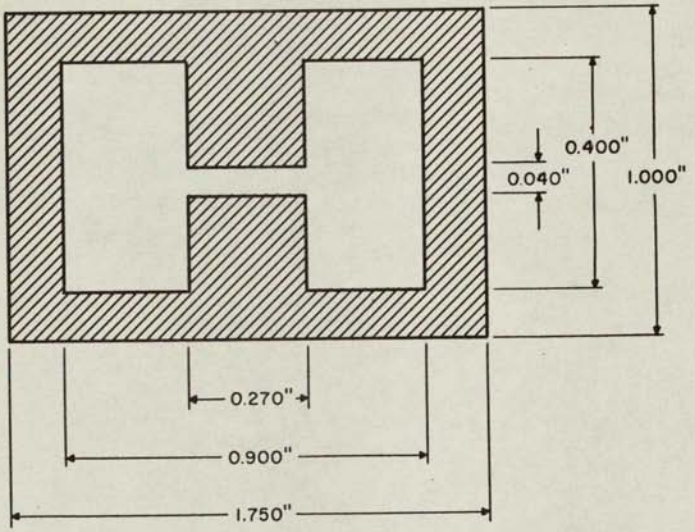

Fig. 9 Cross-Section of Double-Ridge Waveguide

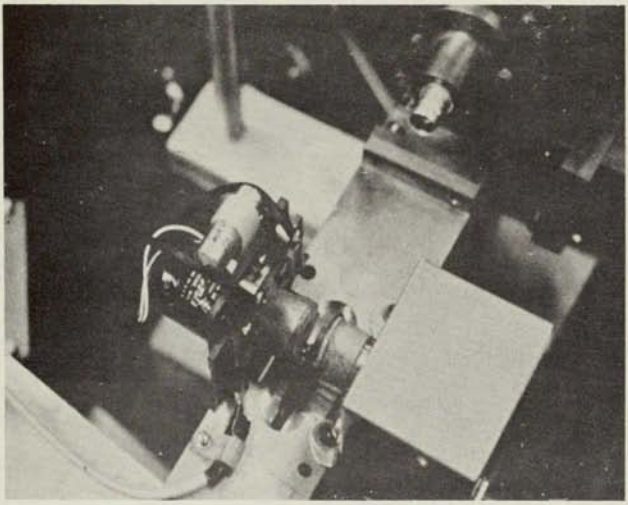

Figure 10. Photograph of Waveguide Switch

the reflection coefficient is fairly low and the longitudinal discontinuity in the guide is not affective on the field lines. Onto the waveguide a motor is mounted with a semicircle resistive card fastened to its rotor. The resistive card is driven in and out of the waveguide through the center slot.

The switching waveguide is also equipped with a photo conductor and a light source. The light source is aligned with the photo conductor which is wired in series with a battery and a resistor. The rotation of the absorbing wheel with the motor produces oscillating voltages across the resistor which are synchronized with the modulation process. This voltage is applied to the reference channel of the phase lock-in amplifier for phase-sensitive detection.

In its present status the mixer arms are satisfactorily matched, but the response over the operation frequency range is not very uniform. However, this is not a lack for the operation of the radiometer since the calibration of the instrument determines the response of the radiometer at each frequency.

The i.f. amplifier circuit is shown in Fig. 11. The input of the amplifier is designed with a transformer whose primary is wired with coils each of an equal number of turns, but opposite in phase. The local oscillator external noise arrives in phase at the balanced arms of the mixer since it is sent through the "H" plane. The primary turns N_1 and N_2 are coiled in opposite directions, and

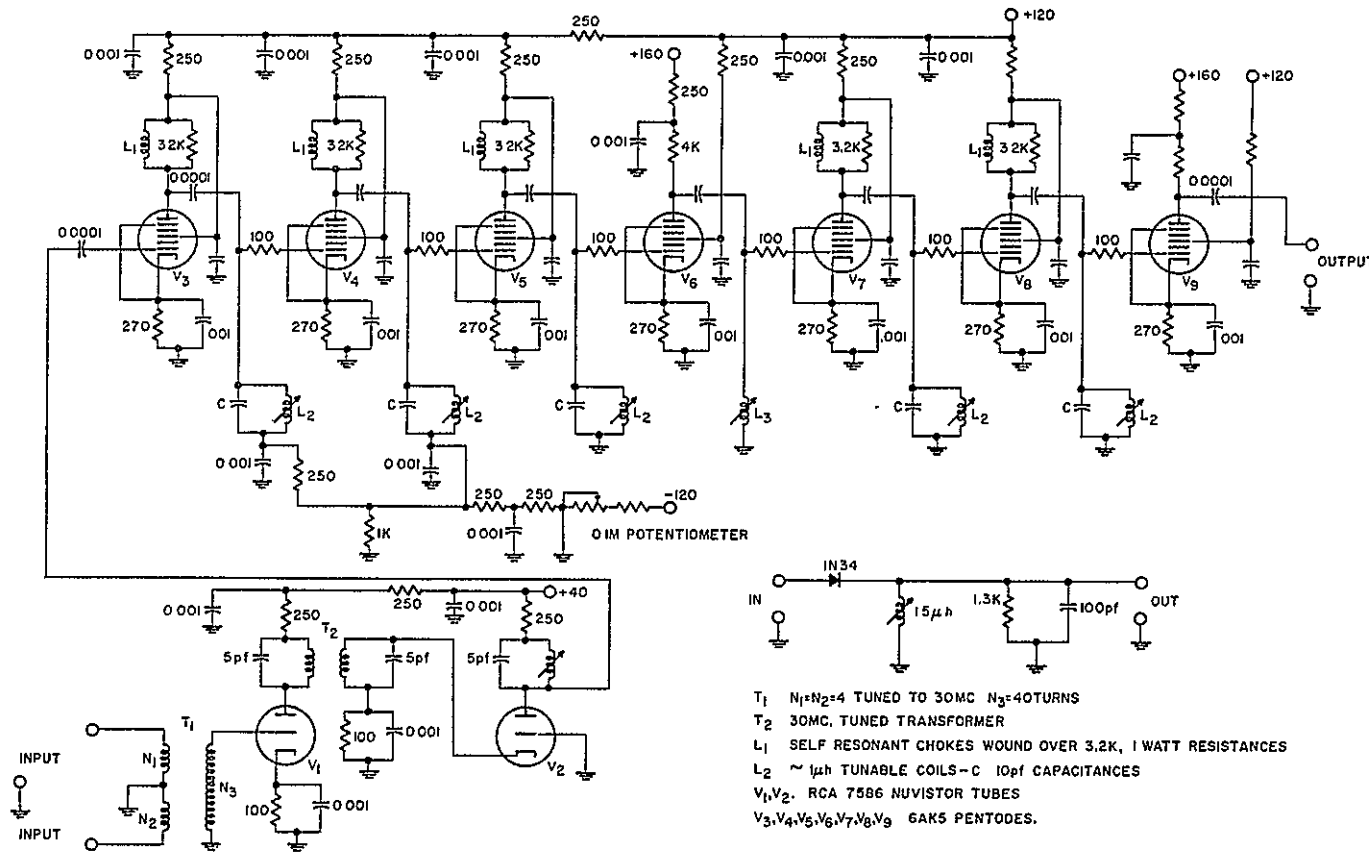

Fig. 11 I.F. Amplifier Circuit, and the Detector

this phase inversion furnishes cancellation of the local oscillator noise at the input of the i.f. amplifier. The transformer at the input stage is useful also in providing an optimum input impedance for the first stage. The noise figure of the amplifier is very much dependent upon its input impedance. With the balanced mixer crystals (1N23WEM) used, there is an effective input impedance of 2400 Ohms to the i.f. amplifier. In Appendix II this value of impedance is shown to minimize the noise figure of the amplifier.[24] The secondary of the input transformer is tuned with the input capacitance of the first stage triode to 30 MC.

The initial stages of the i.f. amplifier are constructed using low noise triode tubes since partition noise is absent in triodes in comparison to pentodes or tetrodes. The first two stages are cascode connected where the grounded-cathode is followed by a grounded-grid triode. The amplification factor of the first stage is low, and this provides a stable grounded-cathode circuit. The transformer between the triodes is used to tune both stages to 30 MC by proper design of the coils. In this cascode arrangement, the noise figure of the grounded-grid stage is small enough so that the noise factor of both triodes is very close to that of the grounded-cathode stage alone.[25]

The detector used at the output of the i.f. amplifier is also shown in Fig. 11. A germanium diode (1N34) is used in the detector

circuit, and its characteristic represents a square law. In order to establish proper matching of the i.f. amplifier to the phase lock-in amplifier, a tunable coil is placed following the detector.

CHAPTER IV

MEASUREMENTS AND CALIBRATION

Following the completion of various parts of the radiometer, the characteristics of some of the components had to be determined before any calibration procedure was attempted. The waveguide switch attenuation, the frequency response and the noise figure of the i.f. amplifier, and the over-all noise figure of the receiver were among some of the measurements made. Once these parameters were specified, the calibration of the radiometer was carried out using three different noise sources at a temperature of 11,000°K. After the calibration of the apparatus a set of cyclotron radiation intensity measurements were made using an argon discharge tube at a pressure of 30 microns with a discharge current of 400 milliamps under about a 1 Kgauss magnetic field.

The switching-waveguide attenuation as a function of frequency is sketched in Fig. 12. The resistive-card power absorption varies between 10 and 15 db depending upon the incident power frequency.

The i.f. amplifier frequency response curve is obtained using an intermediate frequency generator (Fig. 13). The input to the amplifier is kept at a constant value of 10 microvolts, and the frequency of operation is varied. The i.f. amplifier is tuned to 30 MC with a bandwidth of 1.5 MC. By making use of a noise figure

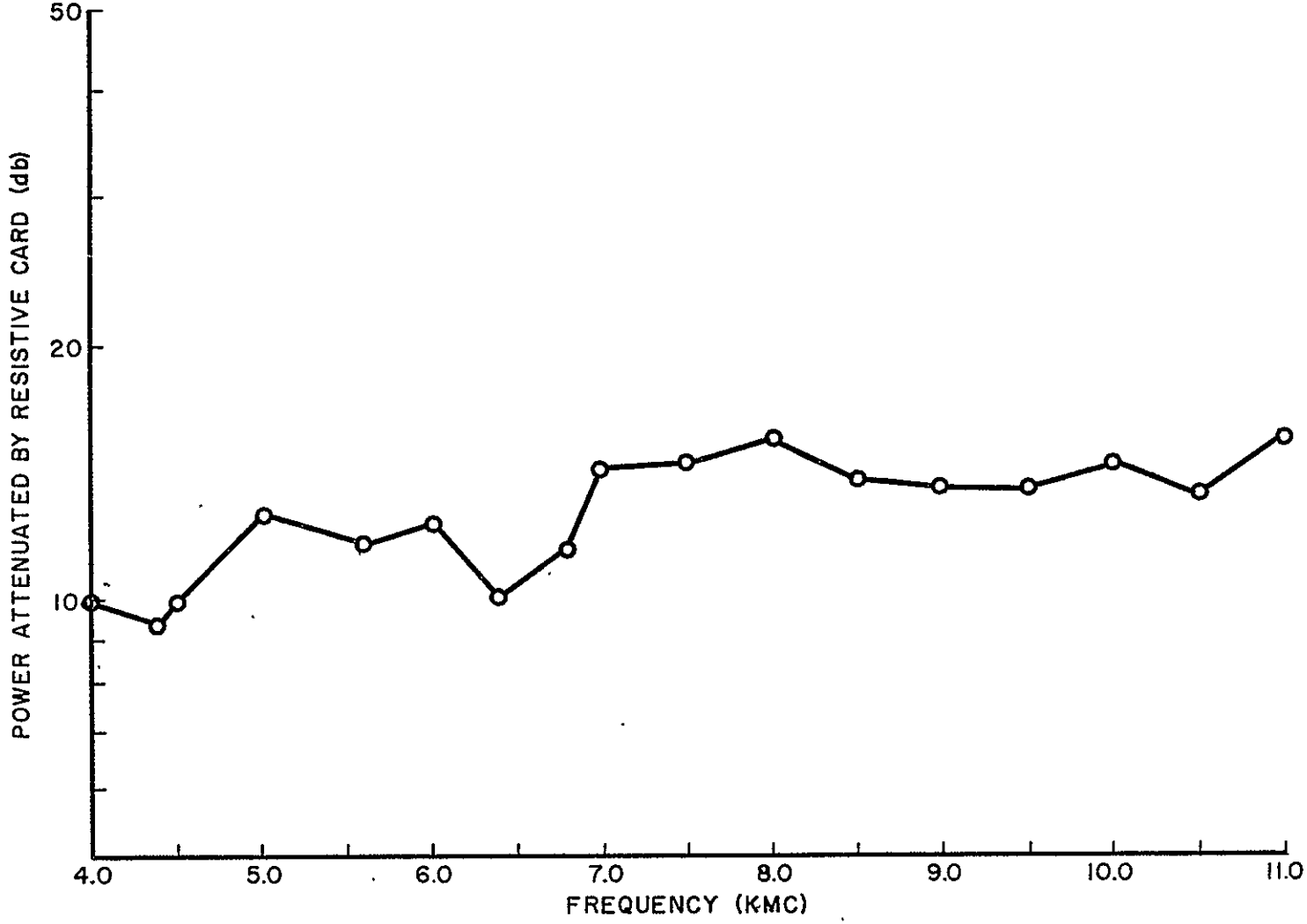

Fig. 12 Switch Attenuation versus Frequency

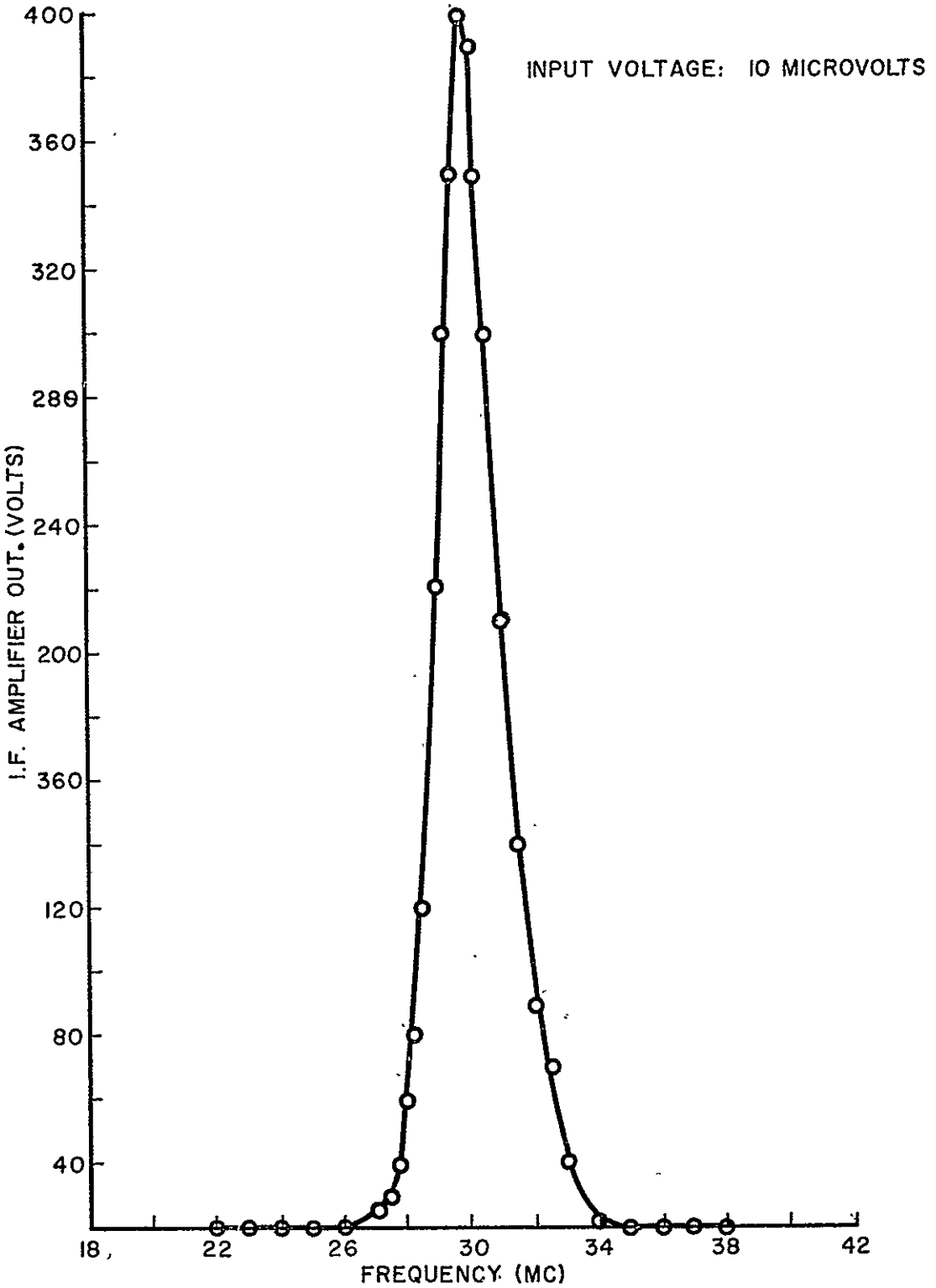

Fig. 13 I.F. Amplifier Output Versus Frequency

meter, the amplifier noise figure of 3 db is also measured.

The radiometer temperature sensitivity as given in Eq. (6) is one of the parameters that has to be specified. Therefore, the overall-noise figure of the receiver needs to be measured. The circuit block diagram for the receiver noise figure measurements is shown in Fig. 14. An X-Band noise source is applied to the input of the radiometer. The output of the i.f. amplifier is connected to a noise-figure meter which measures the relative noise figure automatically. The local oscillator frequency is swept over a small range of X-Band frequencies, and an average receiver noise figure of 16.5 db is measured.

The calibration of the radiometer is carried out using two fluorescent and one argon noise source located inside an S-Band waveguide. The S-Band horn is connected to the input to provide a suitable transition to the double ridged-waveguide. The local oscillator is swept over the frequency range of 2.6 to 9 KMC, and a point by point plot of the radiometer output voltage is made at 50 MC intervals. Normalized plots with all three noise sources are shown in Figures 15, 16, and 17. The fluorescent and argon noise tube outputs are very similar at the lower frequencies. However, above 6 KMC the argon tube output is higher. The voltages sketched on these figures correspond to a temperature of 11,000°K at each frequency. Therefore, the calibration of the radiometer is obtained by a pointwise plot. Following the calibration of the radiometer,

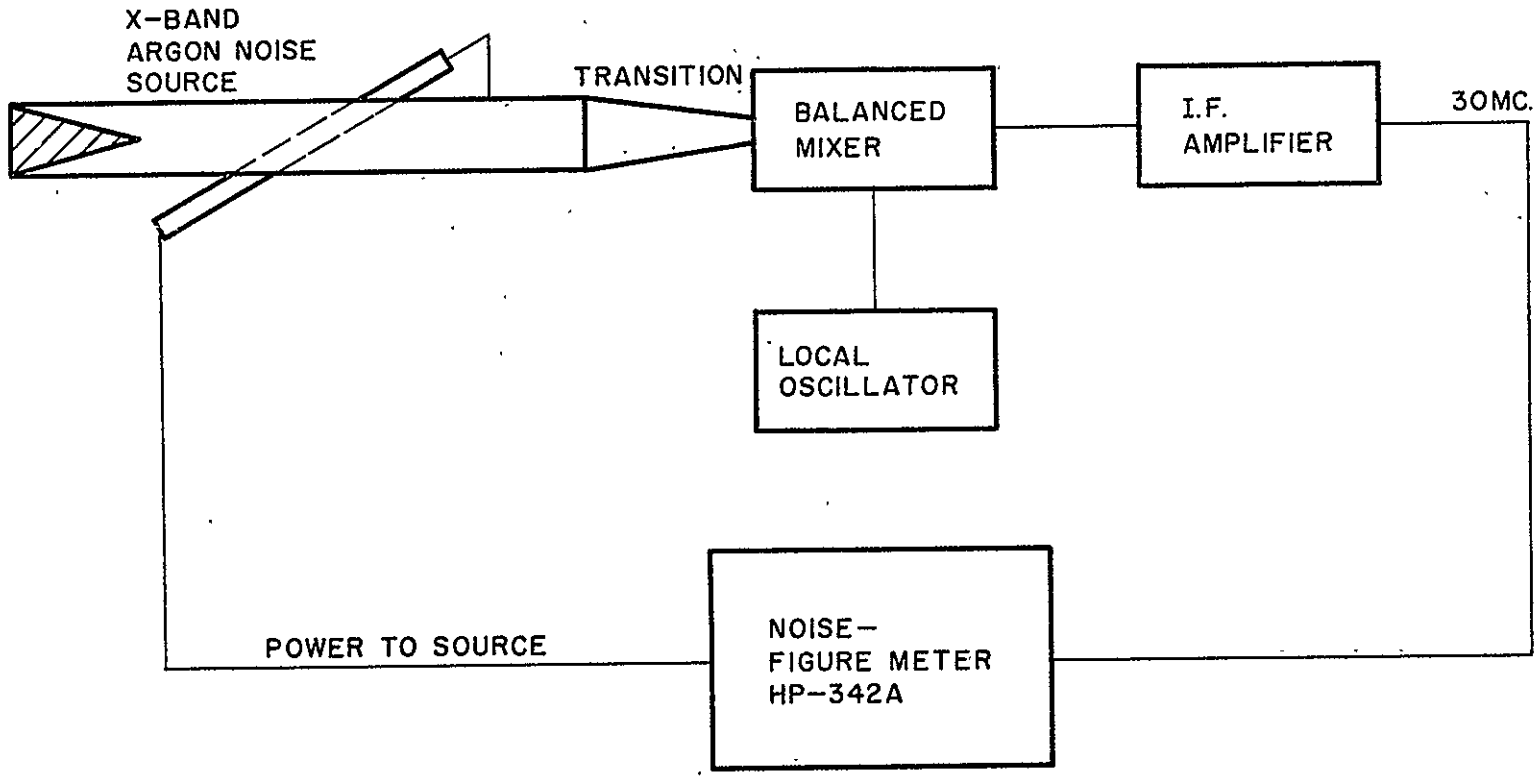

Fig. 14 Receiver Noise-Figure Measurements Block-Diagram

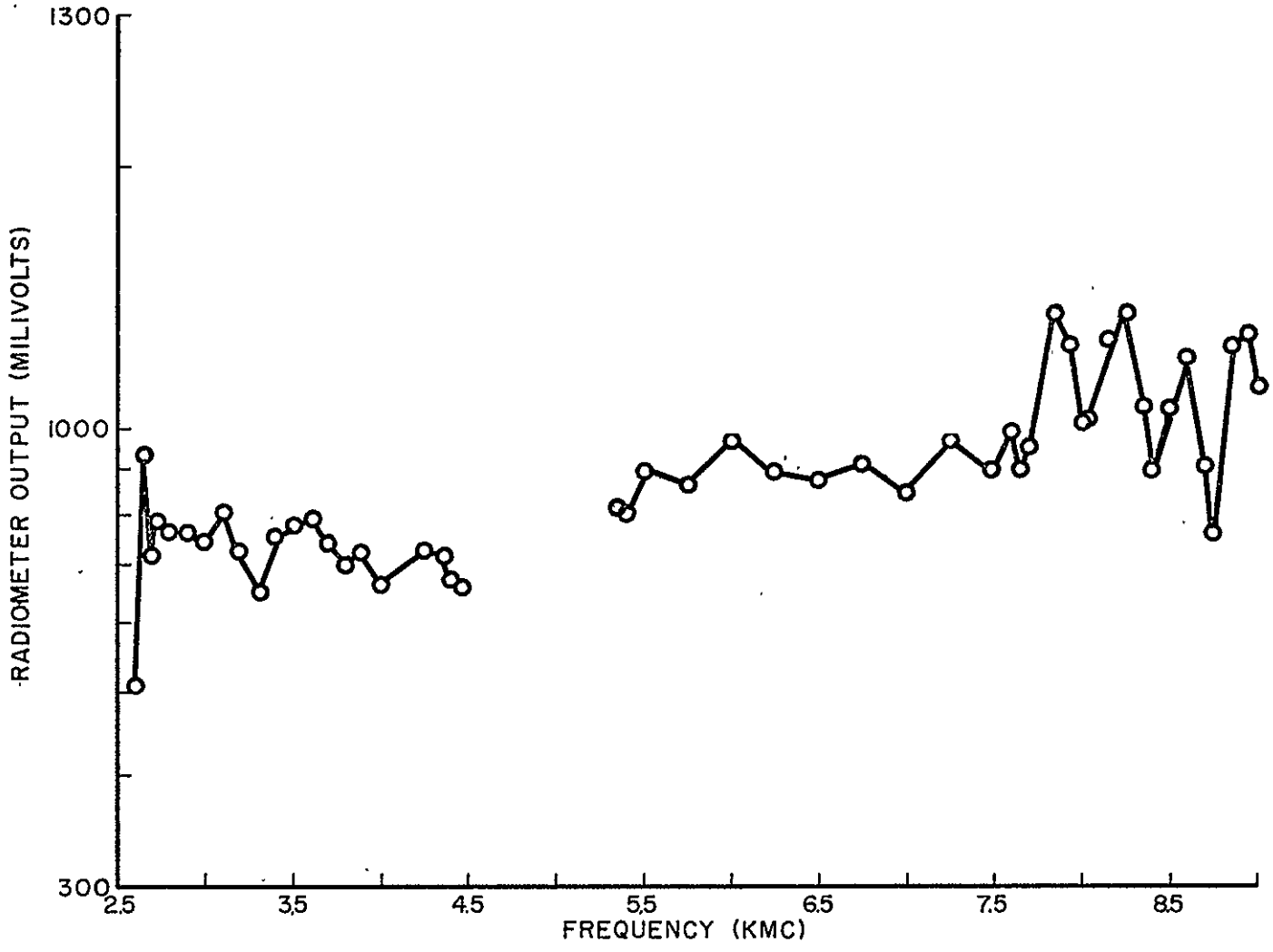

Fig. 15 Argon-Normalized Radiometer Output Versus Frequency

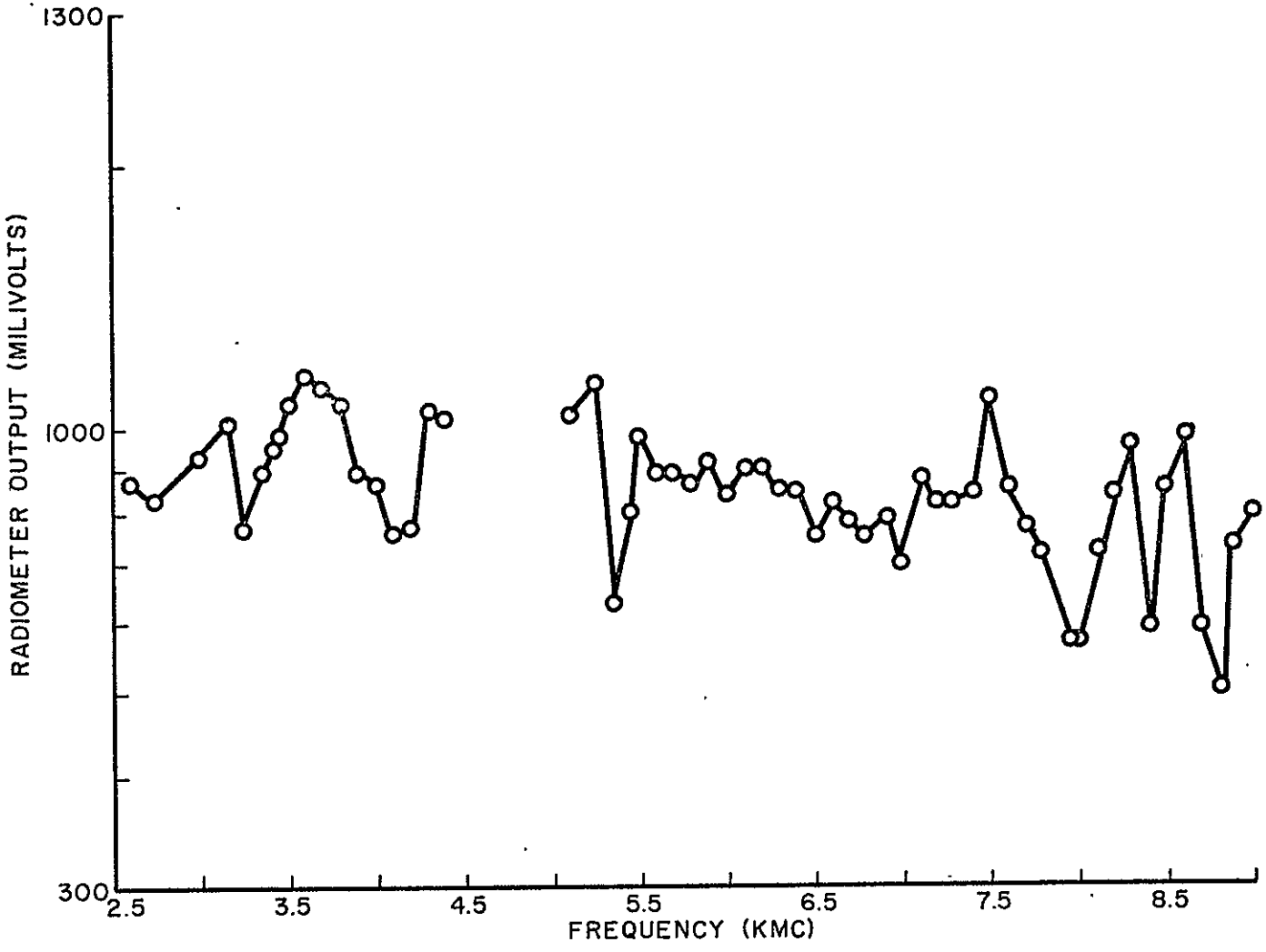

Fig. 16 Fluorescent ^{I} Normalized Radiometer Output Versus Frequency

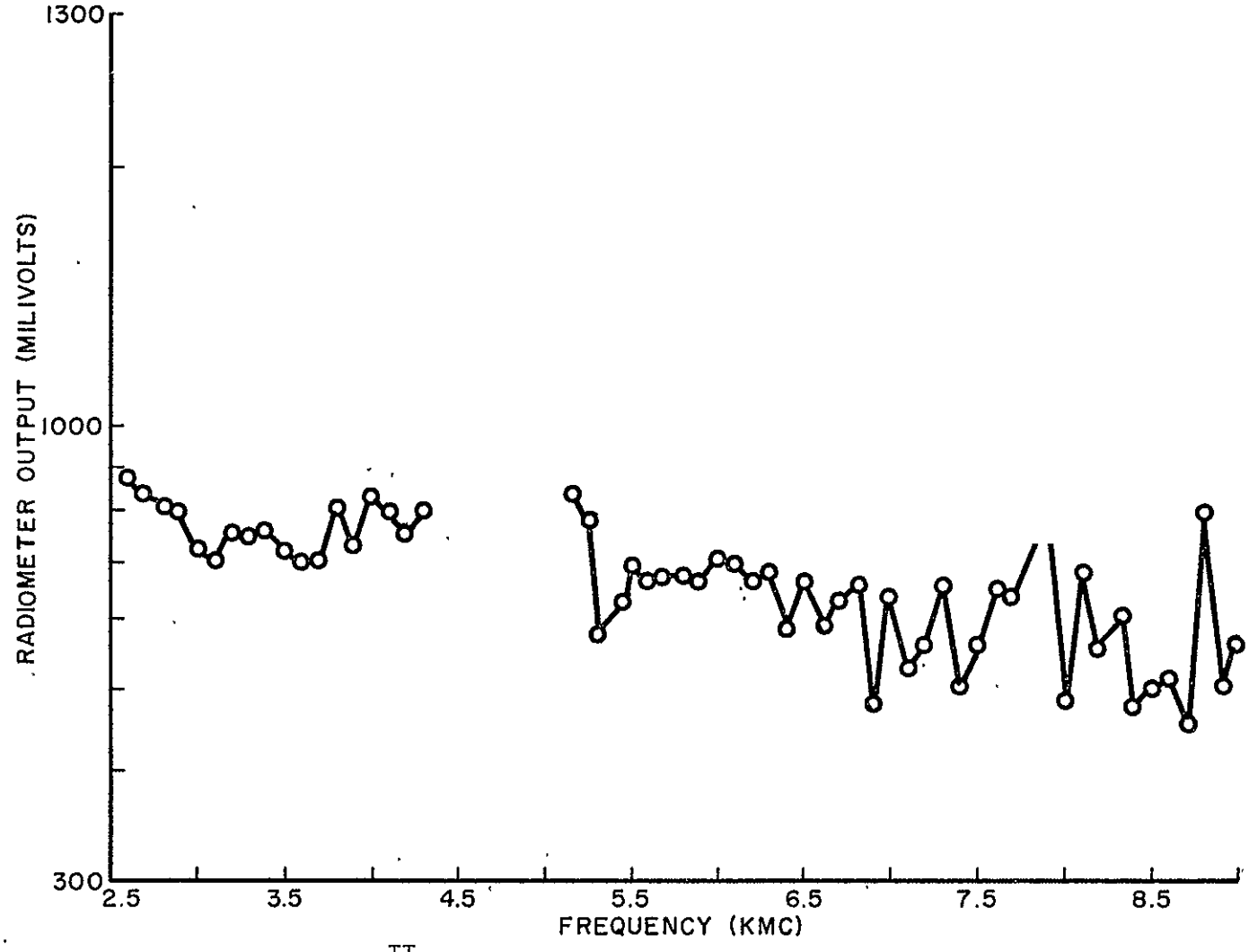

Fig. 17 Fluorescent[II] Normalized Radiometer Output Versus Frequency

the apparatus shown in the block diagram of Fig. 18 is prepared to obtain a set of cyclotron radiation intensity measurements.

It is well-known that an electron in an external magnetic field radiates electromagnetic energy at the cyclotron frequency and at its harmonics. The electron cyclotron frequency is given by

$$\omega_c = \frac{eB_o}{m_e} \tag{9}$$

where B_o is the external magnetic field, and e and m_e are charge and mass of an electron, respectively. An argon discharge tube that is used as a source of radiation is located inside an S-Band waveguide. This waveguide is surrounded by a magnetic coil which establishes a magnetic field parallel to the discharge tube axis and the length of the waveguide. The argon discharge tube pressure is maintained at 30 microns, and a D.C. current of 400 milliamperes is run through it. The magnetic field intensity is about 1 Kgauss corresponding to a fundamental cyclotron frequency below 3 KMC. The harmonics are at integer multiples of the fundamental frequency. By sweeping the local oscillator from 2.6 to 9 KMC, the first three harmonics of the radiation intensities are meaaured. In Fig. 19 the normalized radiometer output voltages for the radiation; is plotted as a function of frequency by selecting points 50 MC apart.

For all the measurements made with the radiometer, the R-C

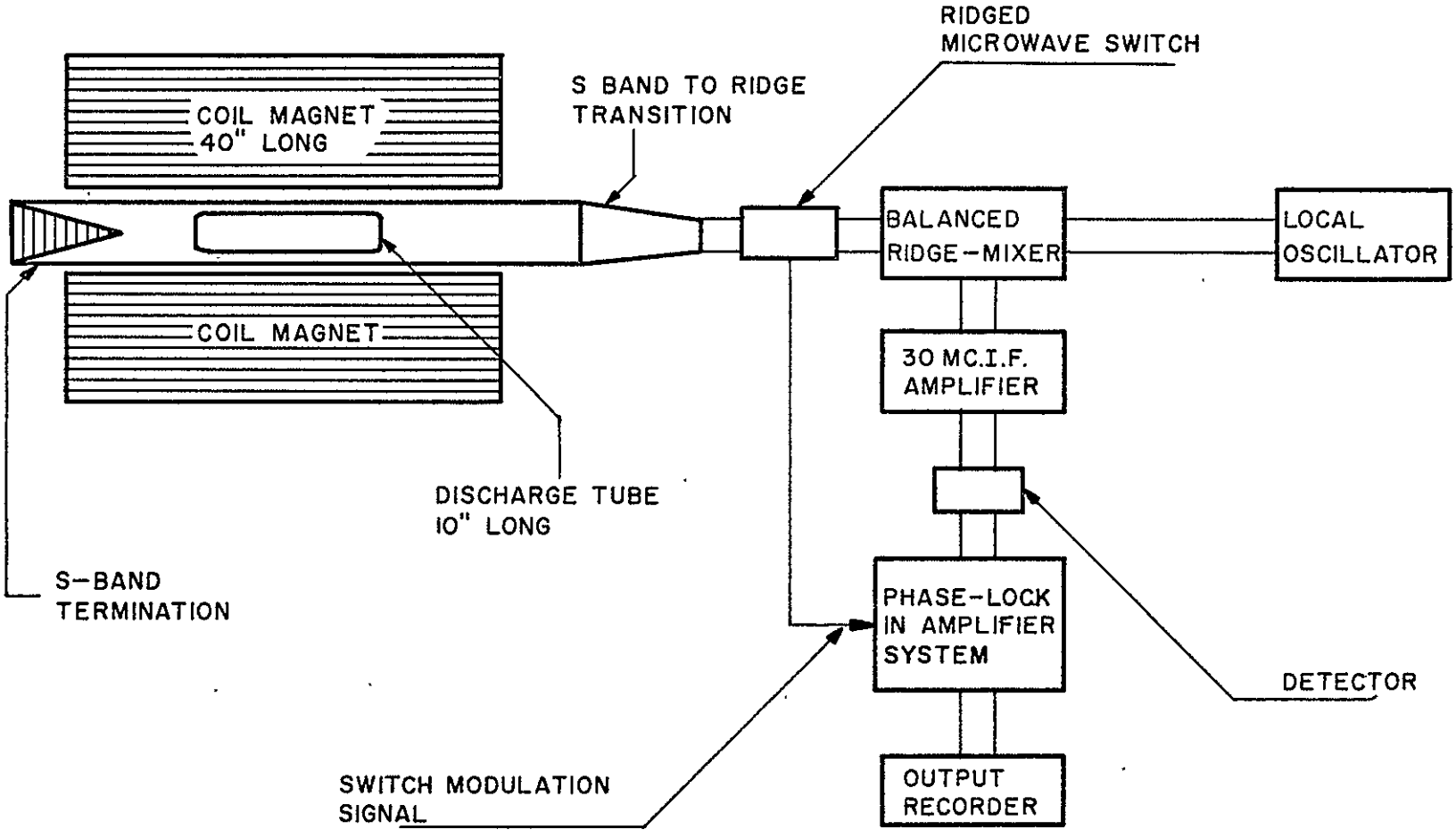

Fig. 18 Block Diagram of the Radiometer Circuit
For Cyclotron Radiation Measurements

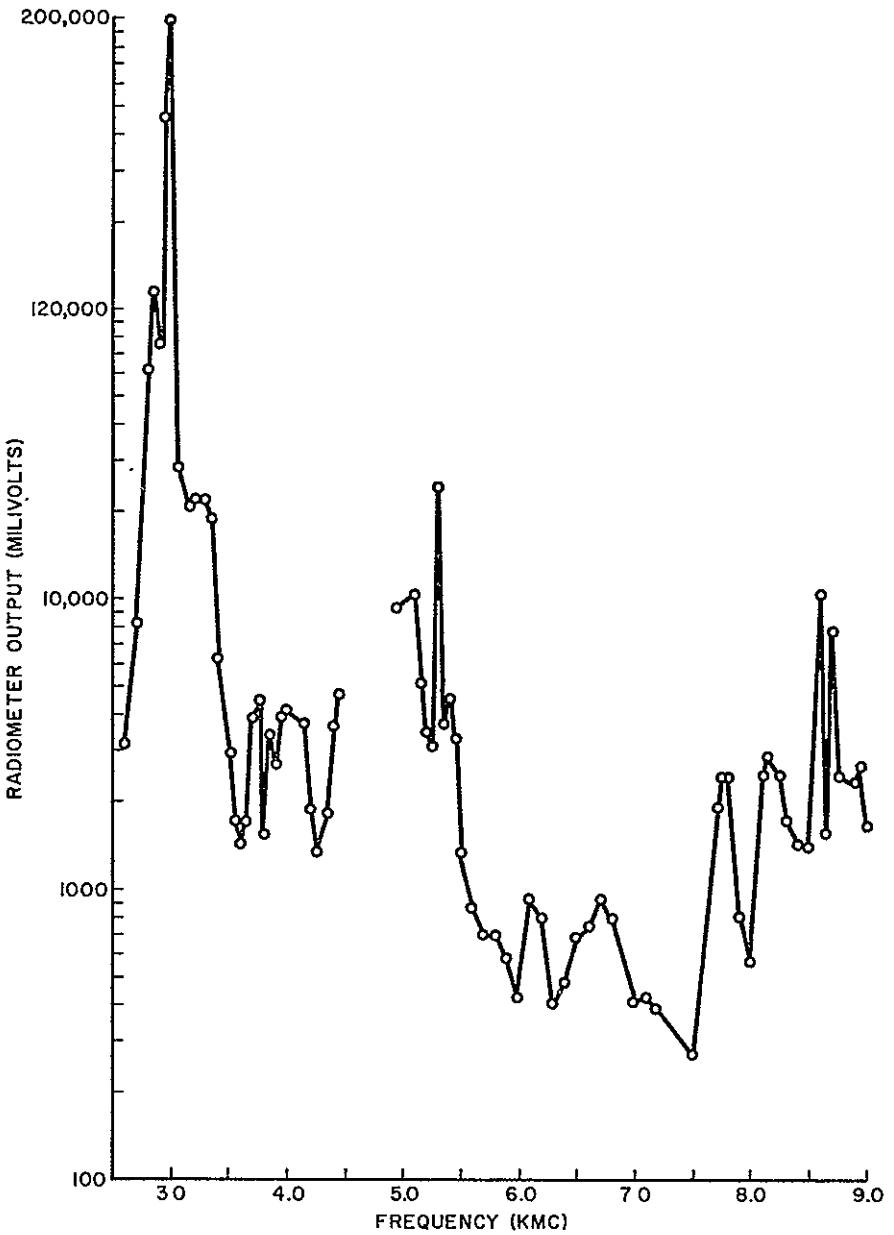

Fig. 19 Cyclotron Radiation - Radiometer Output Versus Frequency

low-pass filter time constant was selected to be $\tau = 3$ seconds. This is equivalent to a filter bandwidth of $\gamma = \frac{1}{3}$ cps. Therefore, the minimum detectable signal of the radiometer can be calculated from Eq. (4), since the i.f. amplifier bandwidth is $\alpha = 1.5$ MC.

$$\sigma_{md}^2 = 2.65 \times 10^{-3} \sigma_n^2 \tag{10}$$

This implies that a signal power which is about 3/1000 of the input noise power can be detected with the radiometer.

The minimum detectable temperature change can also be computed since the receive noise figure and the comparison source temperature are known parameters.

Using Eq. (6),

$$F = 16.5 \text{ db}$$

$$T_a = 300°K$$

$$\gamma = \frac{1}{3} \text{ cps}$$

$$\alpha = 1.5 \times 10^6 \text{ cps} .$$

$$\Delta T = 2.3K \text{ °K} \tag{11}$$

However, for the Dicke radiometer the value of constant K[4,11] is $\frac{\pi^{3/2}}{8} = 0.69$, and therefore,

$$\Delta T \cong 1.6°K . \tag{12}$$

CHAPTER V

DISCUSSION OF THE RESULTS AND THE CONCLUSIONS

The double-ridged balanced mixer used in the radiometer could have been operated from 2.6 to 14 KMC; however, the absence of a microwave signal generator above 9 KMC made it possible to check the instrument above this frequency. Within the frequency range 2.6 to 9 KMC, the mixer arms balanced sufficiently well, but the frequency response was not uniform. The non-uniform frequency response was due to the magic "T" junction where, at certain frequencies, the incident power was only partly transmitted to the mixer crystals. In the frequency range 4.5 to 5 KMC, there was complete reflection of the signal sent through the "E" plane of the mixer. Except for the 0.5 KMC frequency interval between 4.5 and 5 KMC, it was still possible to use the mixer in the radiometer provided frequency characteristics were taken into account during the calibration procedure.

The double-ridged directional coupler built for the radiometer was not used at all because of undesirable variations in the coupling coefficient. This difficulty was faced, mainly because of the double ridges used.

The microwave switch employed was a resistive card driven at 80 cycles per second with about 90% resulting power attenuation.

The slot through which the resistive card was driven in and out of the ridged waveguide did not cause any noticeable discontinuity to the field lines, and the reflection coefficient was always below two. In the original Dicke radiometer, instead of 80 cycles per second, a 30 cycles per second switching frequency was used. Even though the switching time did not appear explicitely in the earlier sensitivity equations (4) and (6), it was a critical factor toward achieving improved sensitivities for the radiometer. This was due to the fact that with high modulation frequency a considerable cancellation of the circuit's inherent noise would take place since, during the switching interval, the inherent noise level would not deviate noticeably. On the other hand, with low switching frequencies if a small quantity of noise remained in the circuit during the switching process, it would appear on the output of the radiometer as fluctuations and effectively would reduce the sensitivity.

The i.f. amplifier used was tuned to 30 MC and had a bandwidth of 1.5 MC. As shown in Equations (4) and (6), the sensitivity of the radiometer was inversely proportional to the square root of the i.f. bandwidth. Therefore a larger i.f. bandwidth than the one used would result in a better sensitivity for the radiometer. However, there had to be an upper bound for the bandwidth of the i.f. amplifier, and this had to be determined by the experiment in which the radiometer was to be used. In the derivation of the sensitivity

expression for the radiometer, the incoming signal was assumed to be uniform over the bandwidth of the receiver, which was equivalent to the i.f. bandwidth. If the signal received at the input of the radiometer had a bandwidth smaller than the radiometer bandwidth, the original assumptions made in Chapter II concerning the signal, in a computation of sensitivity, would be violated. Therefore, partly for this reason, and partly for high gain purposes a 1.5 MC i.f. bandwidth was selected.

The radiometer was calibrated using argon and fluorescent noise sources. However, because of the non-uniform balanced mixer frequency response, the calibration curves shown in Figures 15, 16, and 17 were accordingly normalized. Again due to the imperfect mixer response, there were no calibration points in the frequency interval 4.5 to 5.0 KMC. This was a lack for the operation of the radiometer in this 0.5 KMC frequency interval, but in comparison to the receiver total bandwidth, it was rather negligible part of the operational range.

All of the noise sources used for the calibration of the equipment were at about the same temperature (11,000°K), and the normalized outputs revealed reasonable agreement even though there were discrepancies at some of the frequencies (Figures 15, 16, 17). Part of the discrepancies could be due to the differences between the radiated power intensities of the noise sources in the 2.6 to 9 KMC frequency range. Also, part of the problem was encountered

because of incapable equipment available to keep the local oscillator output power at a constant level. The trouble associated with the local oscillator power output variation with frequency could have been overcome if the double ridge directional coupler had operated satisfactorily.

The measurements made with the radiometer on cyclotron radiation intensities were indicative of just one of the uses of this wide band radiometer. As it can be observed from Figure 19 that the three peaks measured were most likely the radiated harmonics. The fundamental cyclotron frequency was about 2.95 KMC, and this was clearly stressed by a very high radiometer output reading since cyclotron radiation intensity was expected to have a maximum value at the first harmonic.

Radiometers built up to now, as far as it is known from the literature, have been constant frequency or very limited in their bandwidths. Undoubtedly, there are numerous difficulties involved in the construction of a very wide-band radiometer such as the one described in this report. The microwave frequency section of a wide-band radiometer constitutes the bulk of the problems encountered. For example, a uniform frequency response for the balanced mixer and the directional coupler is extremely hard to achieve over the frequency range 2.6 to 14 KMC. A double-ridged magic "T" junction has to be designed in such a way as to accept power equally well from both "E" and "H" planes. Mixer crystals in the balanced

arms have to be matched to the waveguide characteristic impedance in order to assure minimum power reflection. Due to the small ridge gap, which determines the wide-band capability of a double-ridged waveguide, it is also very difficult to obtain satisfactory power coupling in a ridged directional coupler. Proper operation of a ridged directional coupler can be of great importance in the calibration of the radiometer since it enables one to monitor the local oscillator power output continuously throughout the calibration.

The sensitivity of this radiometer can be improved appreciably if, instead of a resistive card, a standard noise source is used in the microwave switching circuit. The resistive card used can only be assumed to be at room temperature (300°K), and any temperature drift of the card can cause variations in the output reading. Through the use of a standard comparison noise source, the temperature of the source can always be monitored to keep it at a constant level. When the temperature of the comparison noise source used in the switching circuit is comparable to the temperature of the object to be studied, the sensitivity of the radiometer again improves.[21] Therefore the use of a standard source in the microwave switching section has advantages, but it requires construction of a different type of switching waveguide. In the use of a standard source, a two-diode switching circuit might be an ideal configuration to use. The diodes would switch the incoming signal on and the comparison

source off simultaneously and vice versa. However, in this case very low forward impedance microwave crystals have to be employed since the characteristic impedance of the double ridge waveguide is considerably low. Of course, operation of a diode switching circuit will also mean an improvement in the sensitivity by about a factor of four since square wave modulation would be possible. (Eq. 5).

Undoubtedly with local oscillators covering the range above 9 KMC, higher cyclotron harmonics can also be measured with this radiometer. Therefore, given a fundamental cyclotron frequency of 2.95 KMC established by the magnetic field, one can measure as high as the fifth harmonic of radiation. In this report only as an application of the radiometer, cyclotron resonance intensity measurements are made and there remains a great deal to be studied on this matter.

APPENDIX I

Referring back to the block diagram of Fig. 4, and the assumptions made in Chapter II, the output of the amplifier is,

$$y(t) = \left[\frac{1 + \text{Sin } 2\pi qt}{2}\right] s(t) + n(t) \tag{13}$$

since the noise voltage n(t) is not affected by the modulation. The square law detector output is related to its input as,

$$x(t) = K[y(t)]^2 \tag{14}$$

where K is a constant, and therefore

$$x(t) = K\left[\left(\frac{1 + \text{Sin } 2\pi qt}{2}\right)^2 s^2(t)\right.$$

$$\left. + (1 + \text{Sin } 2\pi qt)\, s(t)n(t) + n^2(t)\right] \tag{15}$$

At this point, it will be helpful to make use of correlation technique by computing the autocorrelation function of x(t). If we express this correlation function as $R_1(\tau)$, then the spectral density at the output of the detector is,

$$G(f) = \int_{-\infty}^{\infty} R_1(\tau)e^{i\omega t}\, dt \tag{16}$$

where f is the frequency, and τ is the correlation parameter.

The autocorrelation function of x(t) is given as,

$$R_1(\tau) = \lim_{T\to\infty} \frac{1}{2T} \int_{-T}^{T} x(t)x(t+\tau)\, dt \tag{17}$$

The product of x(t) with $x(t + \tau)$ can be expressed in the following way,

$$x(t)x(t+\tau) = K^2\{\frac{s^2(t)s^2(t+\tau)}{16}[1 + \mathrm{Sin}2\pi qt]^2[1 + \mathrm{Sin}2\pi q(t+\tau)]^2$$

$$+ s(t)s(t+\tau)n(t)n(t+\tau)[1 + \mathrm{Sin}2\pi qt][1 + \mathrm{Sin}2\pi q(t+\tau)]$$

$$+n^2(t)n^2(t+\tau) + \frac{1}{4}s^2(t)n^2(t+\tau)(1 + \mathrm{Sin}2\pi qt)^2$$

$$+ \frac{1}{4}s^2(t+\tau)n^2(t)[1 + \mathrm{Sin}2\pi q(t+\tau)]^2\} \tag{18}$$

by neglecting rest of the terms that involve only cross-correlation of noise with the signal, which is zero.

As mentioned in Chapter II (p. 10) the ergodic theorem is assumed to be valid, and the statistical averages are the same as the time averages. It is also known that the statistical average of two independent signals g(t) and f(t) can be separated as multiple of the averages,

$$E[g(t)f(t)] = E[g(t)]E[f(t)] \tag{19}$$

where E indicates the statistical averaging.

Applying expression of eq. (19) to eq. (18), with the following identities,

$$\begin{aligned} E[s^2(t)s^2(t+\tau)] &\equiv \overline{s^2(t)s^2(t+\tau)} \\ E[s(t)s(t+\tau)] &\equiv \overline{s(t)s(t+\tau)} \\ E[n(t)n(t+\tau)] &\equiv \overline{n(t)n(t+\tau)} \\ E[s^2(t)] &\equiv \overline{s^2(t)} \\ E[n^2(t)] &\equiv \overline{n^2(t)} \end{aligned} \tag{20}$$

$R_1(\tau)$ can be written as,

$$R_1(\tau) = K^2\{\frac{\overline{s^2(t)s^2(t+\tau)}}{16}\left[\frac{9}{4} + 2\,\mathrm{Cos}2\pi qt + \frac{1}{8}\,\mathrm{Cos}\,4\pi q\tau\right]$$

$$+ \overline{s(t)s(t+\tau)}\;\;\overline{n(t)n(t+\tau)}\,(1 + \frac{1}{2}\,\mathrm{Cos}\,2\pi q\tau) + \frac{3}{4}\,\overline{n^2(t)}\;\overline{s^2(t)}$$

$$+ \overline{n^2(t)n^2(t+\tau)}\} \qquad (21)$$

From the assumption of the signal and the noise it is true that,

$$\overline{s^2(t)} = \sigma_s^{\,2} = \overline{s^2(t+\tau)}$$

$$\overline{n^2(t)} = \sigma_n^{\,2} = \overline{n^2(t+\tau)} \qquad (22)$$

Using the identities associated with the statistical averages,

$$\overline{s^2(t)s^2(t+\tau)} = \sigma_s^{\,4} + 2[\overline{s(t)s(t+\tau)}]^2 \qquad (23)$$

$$\overline{n^2(t)n^2(t+\tau)} = \sigma_n^{\,4} + 2[\overline{n(t)n(t+\tau)}]^2 \qquad (24)$$

where,

$$\overline{s(t)s(t+\tau)} = \frac{\sigma_s^{\,2}\mathrm{Cos}2\pi f_1\tau\mathrm{Sin}2\pi\alpha\tau}{\pi\alpha\tau} \qquad (25)$$

$$\overline{n(t)n(t+\tau)} = \frac{\sigma_n^2 \text{Cos}2\pi f_1 \tau \text{Sin}2\pi\alpha\tau}{\pi\alpha\tau} \tag{26}$$

Substituting equations 22-26 into eq. 21,

$$R_1(\tau) = K^2\{\frac{\sigma_s^4}{8} \text{Cos } 2\pi q\tau + (\frac{9}{64}\sigma_s^4 + \frac{3}{4}\sigma_n^2\sigma_s^2 + \sigma_n^4)$$

$$+ (\frac{9}{64}\sigma_s^4 + \frac{\sigma_n^2\sigma_s^2}{2} + \sigma_n^4)\frac{\text{Sin}^2\pi\alpha\tau}{(\pi\alpha\tau)^2}$$

$$+ (\frac{\sigma_s^4}{8} + \frac{\sigma_n^2\sigma_s^2}{4})\frac{\text{Sin}^2\pi\alpha\tau}{(\pi\alpha\tau)^2} \text{Cos } 2\pi q\tau\}. \tag{27}$$

In order to find the spectral density, eq. 16 can be used. When the integrations are carried out the following terms are obtained,

$$G_{11}(f) = K^2 \int_{-\infty}^{\infty} \frac{\sigma_s^4}{8} \text{Cos } 2\pi q\tau e^{-j2\pi f\tau} d\tau = \frac{K^2}{8}\sigma_s^4\delta(f-q) \tag{28}$$

$$G_{12}(f) = K^2 \int_{-\infty}^{\infty} (\frac{9}{64}\sigma_s^4 + \frac{3}{4}\sigma_n^2\sigma_s^2 + \sigma_n^4) e^{-j2\pi f\tau} d\tau$$

$$= K^2(\frac{9}{64}\sigma_s^2 + \frac{3}{4}\sigma_n^2\sigma_s^2 + \sigma_n^4)\delta(f) \tag{29}$$

$$G_{13}(f) = K^2 \int_{-\infty}^{\infty} \left(\frac{9}{64}\sigma_s^4 + \frac{\sigma_n^2\sigma_s^2}{2} + \sigma_n^4\right) \frac{\mathrm{Sin}^2\pi\alpha\tau}{(\pi\alpha\tau)^2} e^{-j2\pi f\tau} d\tau$$

$$= K^2\left(\frac{9}{64}\sigma_s^4 + \frac{\sigma_n^2\sigma_s^2}{2} + \sigma_n^4\right) \cdot \begin{cases} 0 & , f > \alpha \\ \frac{2}{\alpha^2}(\alpha - f), & f < \alpha \end{cases} \qquad (30)$$

$$G_{14} = K^2 \int_{-\infty}^{\infty} \left(\frac{\sigma_s^4}{8} + \frac{\sigma_n^2\sigma_s^2}{4}\right) \frac{\mathrm{Sin}^2\pi\alpha\tau}{(\pi\alpha\tau)^2} \mathrm{Cos}\ 2\pi q\tau e^{-j2\pi f\tau} d\tau$$

$$= K^2\left(\frac{\sigma_s^4}{8} + \frac{\sigma_n^2\sigma_s^2}{4}\right) \cdot \begin{cases} 2\left(\frac{\alpha - q}{\alpha^2}\right) & , f < q \\ 2\left(\frac{\alpha - f}{\alpha^2}\right) & , q < f < \alpha - q \\ \frac{\alpha + q - f}{\alpha^2} & , \alpha - q < f < \alpha + q \end{cases} \qquad (31)$$

$G_{11}(f)$ is the signal peaked at the band-pass filter center frequency q. However $G_{12}(f)$ is DC that will not be transmitted through the band-pass filter.

G_{13} and $G_{14}(f)$ are mainly the noise spectra densities, and at the output of the band-pass filter the noise power is given as,

$$P = \int_{q - \beta/2}^{q + \beta/2} (G_{13} + G_{14})\, df \qquad (32)$$

or after carrying out the integration,

$$P = K^2[\frac{17}{32}\sigma_s^4 + \frac{3}{2}\sigma_n^2\sigma_s^2 + 2\sigma_n^4]\frac{\beta}{\alpha} \tag{33}$$

The autocorrelation function of V(t), (output of band-pass filter) is given as,

$$R_2(\tau) = R_1'(\tau) + R_1''(\tau) \tag{34}$$

where $R_1'(\tau)$ is the contribution from the signal, and $R_1''(\tau)$ is the contribution from the noise power P of eq. 33

$$R_1'(\tau) = \int_{q-\beta/2}^{q+\beta/2} G_{11}(f)\ \mathrm{Cos}\ 2\pi f\tau\ d\tau \tag{35}$$

or

$$R_1'(\tau) = \frac{K^2}{8}\sigma_s^4\ \mathrm{Cos}\ 2\pi q\tau \tag{36}$$

On the other hand $R_1''(\tau)$ is given as,

$$R_1''(\tau) = \int_{q-\beta/2}^{q+\beta/2} \frac{P}{\beta}\ \mathrm{Cos}\ 2\pi f\tau\ d\tau \tag{37}$$

or

$$R_1''(\tau) = \frac{K^2}{\alpha}\left[\frac{17}{32}\sigma_s^4 + \frac{3}{2}\sigma_s^2\sigma_n^2 + 2\sigma_n^4\right]\frac{\text{Cos } 2\pi q\tau \text{Sin}\beta\pi\tau}{\pi\tau} \qquad (38)$$

Therefore eq. (34) can be expressed as,

$$R_2(\tau) = \overline{V(t)V(t+\tau)}$$

$$= \frac{K^2}{8}\sigma_s^4 \text{ Cos } 2\pi q\tau$$

$$+ \frac{K^2}{\alpha}\left[\frac{17}{32}\sigma_s^4 + \frac{3}{2}\sigma_s^2\sigma_n^2 + 2\sigma_n^4\right]\frac{\text{Cos } 2\pi q\tau \text{Sin}\pi\beta\tau}{\pi\tau} \qquad (39)$$

The output of the multiplier circuit (w(t)) is given in terms of V(t),

$$w(t) = V(t) \text{ Sin } 2\pi qt \qquad (40)$$

and the autocorrelation function of w(t) is,

$$R_3(\tau) = \overline{w(t)w(t+\tau)}$$

$$= \lim_{T\to\infty} \frac{1}{2T}\int_{-T}^{T} w(t)w(t+\tau)\,dt \qquad (41)$$

Using eqs. (39) and (40),

$$R_3(\tau) = \frac{K^2}{16}\sigma_s^4 \mathrm{Cos}^2 2\pi q\tau + \frac{K^2}{2\alpha}\left[\frac{17}{32}\sigma_s^4 + \frac{3}{2}\sigma_s^2\sigma_n^2 + 2\sigma_n^4\right] \cdot$$

$$\frac{\mathrm{Cos}^2 2\pi q\tau \mathrm{Sin}\pi\beta\tau}{\pi\tau}$$

$$- \frac{1}{2}\lim_{T\to\infty} \frac{1}{2T}\int_{-T}^{T} V(t)V(t+\tau)\mathrm{Cos}\ 2\pi q(2t+\tau)dt \quad (42)$$

The low-pass filter located behind the multiplier will eliminate all of the terms which involve frequencies of the order of q since $\gamma << q$. Therefore the terms which will appear at the output of the low-pass filter are,

$$R_3(\tau) = \frac{K^2}{32}\sigma_s^4 + \frac{K^2}{4\pi\alpha\tau}\left[\frac{17}{32}\sigma_s^4 + \frac{3}{2}\sigma_n^2\sigma_s^2 + 2\sigma_n^4\right]\mathrm{Sin}\beta\pi\tau \quad (43)$$

The first term in eq. (43) is the signal, and the second term is the noise-signal combination, but it is noise dominated.

The spectral density of the signal at the output of the low-pass filter is,

$$G_s = \int_{\infty}^{\infty} \frac{K^2}{32} \sigma_n^4 \, e^{-j2\pi f\tau} \, d\tau = \frac{K^2}{32} \sigma_s^2 \, \delta(f) \tag{44}$$

The spectral density corresponding to the second term of eq. 43 is

$$G_{s-n} = \int_{-\infty}^{\infty} \frac{K^2}{4\alpha} \left[\frac{17}{32} \sigma_s^4 + \frac{3}{2} \sigma_n^2 \sigma_s^2 + 2\sigma_n^4\right] \cdot \frac{\sin\beta\pi\tau}{\pi\tau} \, e^{-j2\pi f\tau} d\tau \tag{45}$$

or

$$G_{s-n} = \begin{cases} \frac{K^2}{2\alpha} \left[\frac{17}{32} \sigma_s^4 + \frac{3}{2} \sigma_n^2 \sigma_s^2 + 2\sigma_n^4\right] & f < \frac{\beta}{2} \\ 0 & f > \frac{\beta}{2} \end{cases} \tag{46}$$

Therefore the signal, and the noise powers corresponding to the spectral densities of eqs. (44) and (46) are,

$$\begin{aligned} P_s &= \frac{K^2}{32} \sigma_s^4 \\ P_n &= \frac{K^2}{2} \left[\frac{17}{32} \sigma_s^4 + \frac{3}{2} \sigma_s^2 \sigma_n^2 + 2\sigma_n^4\right] \frac{\gamma}{\alpha} \end{aligned} \tag{47}$$

Then, the ratio of the signal power to the noise power at the output of the low-pass filter is,

$$\left(\frac{S}{N}\right)_o = \frac{\frac{\sigma_s^4}{16}}{\frac{17}{32} \sigma_s^4 + \frac{3}{2} \sigma_n^2 \sigma_s^2 + 2\sigma_n^4} \left(\frac{\alpha}{\gamma}\right) \tag{48}$$

APPENDIX II

CALCULATION OF OPTIMUM INPUT IMPEDANCE FOR MINIMUM NOISE FIGURE

All sources of noise within first stage of an amplifier can be represented by a single source of noise in the input impedance. The noise figure of the first stage is defined as the ratio of total mean square noise voltage produced across the output terminals of the tube, to the mean square noise voltage produced by a thermal noise generator associated with the input source conductance G_s .

Derivation of the first stage noise figure is confined to "single-frequency" approach, where the available noise powers are expressed in an infinitesimal frequency df .

There are mainly four sources of first stage noise. The first one is due to the input conductance G_s with available current i_s . The second source is maintained by the network losses and the ohmic losses with effective current i_1 . The third source is due to noise across the grid-cathode terminals presented by current i_g . And the last one come from the noise across the plate-cathode terminals determined by current i_p . All of these sources are assumed to be statistically independent, and the total mean square voltage across the output terminals of the first tube is,

$$\overline{e_n^2}df = (\overline{i_s^2} + \overline{i_1})|Z_1|^2df + \overline{i_g^2}|Z_2|^2df + \overline{i_p^2}|Z_3|^2df \qquad (49)$$

where Z_1, Z_2, Z_3 are the corresponding impedances. However the mean square noise voltage produced by an ideal amplifier is,

$$\overline{e_s^2}df = \overline{i_s^2}|Z_1|^2df \qquad (50)$$

Therefore the single frequency noise figure of the first stage is,[24]

$$F_1 = 1 + \frac{\overline{i_1^2}}{\overline{i_s^2}} + \frac{\overline{i_g^2}}{\overline{i_s^2}}\frac{|Z_2|^2}{|Z_1|^2} + \frac{\overline{i_p^2}}{\overline{i_s^2}}\frac{|Z_3|^2}{|Z_1|^2} \qquad (51)$$

For effective source temperature of T,

$$\begin{aligned}
\overline{i_s^2}df &= 4KT\,G_s df \\
\overline{i_1^2}df &= 4KT\alpha G_1 df \\
\overline{i_g^2}df &= 4KT\beta G_\tau df \\
\overline{i_p^2}df &= 4KT\,R_{eq.}\,g_m^2 df
\end{aligned} \qquad (52)$$

where G's are equivalent conductances, $R_{eq.}$ is the equivalent noise resistor of the tube, α and β are constants, and g_m is the transconductances of the tube. Then Eq. (51) can be written as,

$$F_1 = 1 + \frac{\alpha G_1}{G_s} + \frac{\beta G_\tau}{G_s} |a|^2 + \frac{g_m^2 R_{eq.}}{G_s} |b|^2 \qquad (53)$$

where

$$a = \frac{Z_2}{Z_1} \quad , \qquad b = \frac{Z_3}{Z_1} \quad .$$

When the tube transconductance satisfies the inequalities,

$$\begin{aligned} g_m &>> G_\tau \\ g_m &>> G_s \end{aligned} \qquad (54)$$

and

$$\begin{aligned} g_m^2 |b|^2 &= |Y_s + G_\tau|^2 \\ |a| &\cong 1 \end{aligned} \qquad (55)$$

where $Y_s = G_s + G_1 + jY_1$, is the total input admittance; Eq. (53) becomes

$$F_1 = 1 + \frac{\alpha G_1}{G_s} + \frac{\beta G_\tau}{G_s} + \frac{R_{eq.}}{G_s} |Y_s + G_\tau|^2 \qquad (56)$$

The value of G_s that will minimize the noise figure F_1 , can be determined by differentiating F_1 with respect to G_s and equating it to zero.

$$\frac{\partial F_1}{\partial G_s} = - \frac{\alpha G_1 + \beta G_\tau + R_{eq.} [(G_1 + G_\tau)^2 + Y_1^2]}{G_s^2} + R_{eq.} = 0 \qquad (57)$$

and

$$G_{s,opt.}^2 = \frac{\alpha G_1 + \beta G_\tau + R_{eq.}[(G_1 + G_\tau)^2 + Y_1^2]}{R_{eq.}} \tag{58}$$

However, the last term in the numerator is much smaller than the first two. Therefore,

$$G_{s,opt.} = \sqrt{\frac{\alpha G_1 + G_\tau}{R_{eq.}}} \tag{59}$$

For the vacuum tube used, the typical values of α, β, G_1, G_τ and $R_{eq.}$ are given as,[24]

$$\begin{aligned} \alpha &\cong 1 \\ \beta &\cong 5 \\ G_1 &\cong 10 \text{ micromhos} \\ G_\tau &\cong 12 \text{ micromhos} \\ R_{eq.} &\cong 385 \text{ ohms} . \end{aligned} \tag{60}$$

Then the optimum input conductance is,

$$G_{s,opt.} = 4.2 \times 10^{-4} \text{ mhos} \tag{61}$$

or the equivalent input impedance is,

$$R_{s,opt.} \cong 2400 \text{ ohms} . \tag{62}$$

LIST OF REFERENCES

1. G. Bekefi, J. D. Coccoli, E. B. Hooper, and S. J. Buchsbaum, Physical Review Letters, vol. 9, no. 1, 6 (1962).

2. Seymour, B. Cohn, Proc. IRE, vol. 35, 783 (1947).

3. Roger S. Colvin, IRE Wes. Con., vol. 3, pt. 8, 52 (1958).

4. R. H. Dicke, Rev. Sci. Instr., vol. 17, 268 (1946).

5. F. D. Drake and H. I. Ewen, Proc. IRE, vol. 46, no. 1, 53 (1968).

6. K. Fujimoto, IEEE Transc. MTT 12, no. 2, 203 (1964).

7. Janis Galejis, Proc. IRE, vol. 45, no. 10, 1420 (1957).

8. William J. Getsinger, IRE Transc. MTT 41, (1962).

9. S. J. Goldstein, Proc. IRE, Vol. 43, 1663, (1955).

10. M. Graham, Proc. IRE, vol. 46, 1966 (1958).

11. D. B. Harris, Microwave J., vol. 3, no. 4, 41, 47 (1960).

12. A. F. Harvey, "Microwave Engineering," Academic Press; London and New York, 1963.

13. Samuel Hopfer, IRE Transc. MTT, 20 (1955).

14. E. J. Kelly, D. H. Lyons, and W. L. Root, Journal of Soc. Indust. Appl. Math., vol. 11, no. 2, 235 (1963).

15. G. Landauer, J. Nuc. Energ., Part C, vol. 4, 395, Pergamon Press Ltd. (1962).

16. Peter Lubell, and P. Levine, Electronics, 51 (Oct. 1962).

17. T. P. Merrit, and F. F. Hall, Proc. IRE, vol. 47, no. 9, 1435 (1959).

18. W. Selove, Rev. Sci. Instr., vol. 25, 120 (1954).

19. G. C. Southworth, J. Frank. Inst. 239, 285 (1945).

20. Leland D. Strom, Proc. IRE, vol. 45, 1291, 1631 (1957).

21. Peter D. Strum, Proc. IRE, vol. 46, no. 1, 43 (1958).

22. W. C. Taft, K. C. Stotz, E. H. Holt, IEEE Transc. Instr. Meas. 90 (1963).

23. D. G. Tucker, M. H. Graham, S. J. Goldstein, Proc. IRE, vol. 45, no. 3, 365 (1957).

24. George E. Valley, Henry Wallman, "Vacuum Tube Amplifiers," Boston Technical Lithographers, Inc., Lexington, Mass. 1946.

25. Henry Wallman, Alan B. Macnee, C. P. Gadsden, Proc. IRE, vol. 36, no. 6, 700 (1948).